AFCRL - 68-0249

ADTEC

THEORETICAL AND EXPERIMENTAL INVESTIGATION OF FOCAL PLANE ADAPTIVE ANTENNA TECHNIQUES

BY

MARVIN COHN AND ROBERT S. LITTLEPAGE

ADVANCED TECHNOLOGY CORPORATION

1830 YORK RD.

TIMONIUM, MARYLAND 21093

Contract No. F19628-67-C-0299
Project No. 4600, 8683
Task No. 460010, 868303
Work Unit No. 46001001, 86830301

FINAL REPORT
Period Covered: 1 April 1967 to 31 March 1968
April 1968

Contract Monitor: Otho E. Kerr
Microwave Physics Laboratory

PREPARED

FOR

AIR FORCE CAMBRIDGE RESEARCH LABORATORIES
OFFICE OF AEROSPACE RESEARCH
UNITED STATES AIR FORCE
BEDFORD, MASSACHUSETTS 01730

AFCRL - 68-0249

THEORETICAL AND EXPERIMENTAL INVESTIGATION OF FOCAL PLANE ADAPTIVE ANTENNA TECHNIQUES

by

Marvin Cohn and Robert S. Littlepage

ADVANCED TECHNOLOGY CORPORATION
1830 York Road
Timonium, Maryland 21093

Contract No. F19628-67-C-0299
Project No. 4600, 8683
Task No. 460010, 868303
Work Unit No. 46001001, 86830301

FINAL REPORT
Period Covered: 1 April 1967 to 31 March 1968
April 1968

Contract Monitor: Otho E. Kerr
Microwave Physics Laboratory

Prepared for

AIR FORCE CAMBRIDGE RESEARCH LABORATORIES
OFFICE OF AEROSPACE RESEARCH
UNITED STATES AIR FORCE
BEDFORD, MASSACHUSETTS

ABSTRACT

A scalar analysis has been performed to determine the field structure in the focal region of apertures focused in their near field ($f/D < 1$). Solutions are given for plane waves at normal incidence, and several selected angles of arrival. The results indicate a substantial variation from the Fraunhofer far field patterns. Because it is a scalar approach, it is limited to large apertures ($D >> \lambda$) and small diffraction angles.

An experiment was designed to complement the analysis. The qualitative agreement is very good. Sources of experimental error have been found which account for the quantitative variations.

A technique for determining the field structure in the focal region, due to a reasonably arbitrary distribution in the aperture plane, is given. It consists of the superposition of an ensemble of plane waves, whose amplitude, relative phase, and angle of arrival are determined by the aperture plane distribution.

TABLE OF CONTENTS

LIST OF ILLUSTRATIONS

LIST OF ILLUSTRATIONS (Continued)

BLANK PAGE

1. INTRODUCTION

The objective of this effort was to develop a manageable mathematical expression for the phase and amplitude distribution in the focal region of a large aperture antenna for a reasonably arbitrary distribution in the aperture plane. The aperture plane distribution is to be considered the result of either reflector surface errors or atmospheric induced errors. Any time varying nature of the aperture plane distribution was not be to considered. The result of the increased understanding of the focal region fields can be used to improve antenna efficiency by; (1) either the design of an improved single feed element or (2) an array of feed elements.

The combined effect of atmospheric turbulence, multipath, and reflector errors results in extremely complicated equivalent aperture distributions. However, regardless of the complexity of the distribution, a Fourier analysis can be used to reduce the problem to a superposition of plane waves with appropriate phase and amplitude. Because the errors are in general not periodic, a Fourier integral would be required. By the nature of atmospheric induced errors, and for reasonably good reflecting surfaces, most of the available energy will be confined to the low order waves. Hence, we will be dealing with the superposition of some reasonable number of waves.

Once the aperture distribution has been synthesized by an ensemble of plane waves, one must treat the diffraction problem for each individual wave. This amounts to finding the correct transform function for the particular aperture.

The exact solution of the electromagnetic boundary value problem for diffraction of a wave at an aperture in an opaque screen,

or (by invoking Babinet's principle of complementary screens) diffraction by a perfectly conducting surface, is quite tedious. Varying degrees of approximation have been applied by many investigators. These range in refinement from the simple scalar Fourier transformation, resulting from the application of far field approximations in the Fresnel-Kirchhoff integral, to the vector treatment of Debye-Picht-Luneberg[1] with integral solutions by the method of stationary phase.

When the diffracting aperture has focal properties, the problem is even more interesting. This is the case that is applicable to the paraboloidal and spherical reflecting antennas. Until recently, most antenna designers assumed that the diffraction pattern in the focal plane of the dish was given by the Fourier transformation of the illumination function. In other words, the field structure in the focal plane has all the properties of the far field. Sherman[2] has shown that this is the case in the Fresnel region. More recent analyses[3] and experiments[4] have indicated that this is not the case for apertures focused in

---

1. Kline, M. and Kay, I., Electromagnetic Theory and Geometrical Optics, Interscience, New York (1965), Chs. XI and XII.
2. Sherman, John W., "Properties of Focused Apertures in the Fresnel Region," IRE Trans. on Antennas and Propagation, Vol. AP-10, No. 4; July 1962.
3. Hyde, Geoffrey, "Transverse Focal Region Fields of a Spherical Reflector," Radio Corporation of America, Scientific Report No. 2 on AFCRL Contract No. AF 19(628)-2758; January 1966.
4. Loux, P.C., Smilen, L.I., and Martin, R.W., "Transverse Antenna Feed Study," Sperry Gyroscope Company, Final Report on AFCRL Contract No. AF 19(628)-2759; January 1966.

their near field (small focal length to diameter ratios). Since most antennas used at radio frequencies are designed with $\frac{f}{D}$'s from .25 to .50, it is particularly important that the diffracted fields be well understood in order to design proper feeding structures.

The key word in the definition of this study is "manageable". It is desired to develop a tool for designing antenna feed systems. There is a scale associated with understanding the focal plane fields. Proceeding from the Fraunhofer approximation, one moves toward an exact understanding by various refinements of the analytical technique. In terms of actual feed design, this scale has a point of diminishing return. Lacking the exact analysis, the merit of any approach rests on its agreement with experiment.

This study has proceeded on the basis of two basic restrictions; (1) it will be assumed that all the apertures of interest are very large ($D >> \lambda$), and (2) it will be assumed that the range of diffraction angles of interest is relatively small. It is difficult to put an absolute limit on the latter condition. Since the goal is to develop methods of designing feed structures, the extent over which physical structures can be located will be limited by the incurred aperture blockage. Hence, knowledge of the fields far from the aperture axis is not required. Another advantage of the small angle limitation is that most of the available energy is in the principal polarization. A vector treatment of the problem may be an unnecessary complication. The key parameter which must be retained in any analytical approach is the effect of very small $\frac{f}{D}$. We have accomplished this by a more rigorous solution of the Fresnel-Kirchhoff integral. This analysis is given in Section 2.

The analysis has been performed for circular and rectangular apertures. Since the range of applicability is to be determined by experiment, it was felt that a one dimensional aperture offered a simplification for the initial study. For this reason, an exact solution of the Fresnel-Kirchhoff integral equation was performed for a focused infinite slit. This geometry, commonly used in optics, has an excellent long wavelength analog in the parallel plate-lens structure. The details of the structure, and the results of the measurements, are given in Section 3.

2. ANALYSIS

It is felt that, for the majority of antennas of interest, much physical insight can be gained by a more rigorous application of the scalar diffraction theory. This approach neglects polarization effects and hence is only applicable to; (1) the principal polarization in the region of the geometric axis of very large diameter antennas, or (2) for structures which by design permit only a single polarization. The analysis is applicable to a very large class of antennas even if we limit the aperture size to fifty wavelengths or greater ($D/\lambda \geq 50$). It has been shown[5] [6] that for apertures as large as this, the boundary wave due to edge effects has a negligible contribution at moderate diffraction angles, and the Fresnel-Kirchhoff integral represents an excellent approximation to the diffracted fields. For a two dimensional aperture (three dimensional diffraction problem), this integral has the form,

$$U_P = \frac{1}{4\pi} \oint_S \left[\frac{e^{ikr}}{r} \nabla U_S - U_S \nabla \frac{e^{ikr}}{r} \right] \cdot \hat{n} dS, \qquad (1)$$

where

U_P = wave disturbance at the observation point

U_S = wave disturbance at the source point

$\frac{e^{ikr}}{r}$ = Huygen spherical sources in the aperture.

---

5. Wolf, E. and Marchand, E.W., "Comparison of the Kirchhoff and the Rayleigh-Sommerfeld Theories of Diffraction at an Aperture," J. Opt. Soc. Am., 54, 587 (1964).

6. Schivering, F., "On the Range of Validity of Fresnel-Kirchhoff's Approximation Formula," IRE Trans. on Antennas and Propagation, Vol. AP-10, No. 1; January 1962.

U_S and $\nabla U_S \cdot \hat{n}$ are taken to be zero everywhere on S except over the region of the aperture. Hence, the integral over the closed surface S reduces to an integral over the aperture. The geometry associated with Equation (1) is shown in Figure 1.

Some simplications can be made to Equation (1), based on the size of the aperture but irrespective of its particular geometry. Consider the term

$$\nabla \frac{e^{ikr}}{r} = \left[-\frac{1}{r} + ik \right] \frac{e^{ikr}}{r} \hat{r} \ . \qquad (2)$$

For the apertures of interest, one can define a range of possible values for the diameter (D), focal length (f), and for the magnitude of the position vector r;

$$50 \leq \frac{D}{\lambda}$$

$$\frac{f}{D} = 0.25$$

$$r \geq f \ .$$

Considering the poorest case, one still finds that $k >> {}^{1}/r$ by an amount $6.283 >> 0.08$. Hence, it is reasonable to neglect the term $-{}^{1}/r$ in Equation (2).

We can make some generalizations about the form of U_S. The focusing properties of the aperture will require the inclusion of some phase distribution (a function of the aperture geometry) such that the fields due to every Huygen source add in phase at some distance f along the aperture axis, for a wave with normal incidence at the aperture. The incident field which satisfies these conditions has the form

$$U_S = E_o \, e^{i\vec{k} \cdot \vec{r}' + ik\delta} \ , \qquad (3)$$

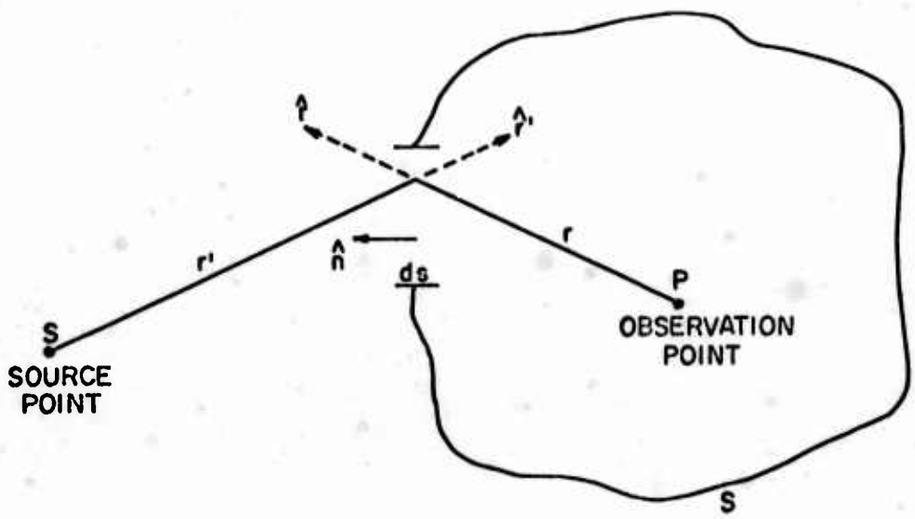

FIG. 1 - DEFINITION OF PARAMETERS IN FRESNEL-KIRCHHOFF EQUATION

where

$\vec{k}$ = incident wave vector

$k\delta$ = phase distribution required for focusing.

Equation (1) can now be written in a form applicable to the three dimensional problems of interest;

$$U_P = \frac{E_o}{4\pi} \iint \frac{e^{ikr}}{r} \left[\nabla e^{i\vec{k}\cdot\vec{r}' + ik\delta} - ike^{i\vec{k}\cdot\vec{r}' + ik\delta} \hat{r} \right] \cdot \hat{n} dS \quad . \tag{4}$$

It should be noted that the mechanism for including the focusing property of the aperture is quite arbitrary. It is not restricted to any particular physical structure such as a lens or shaped reflector. Equation (4) has been studied for circular and rectangular apertures.

2.1 Solution of Equation (4) for a Circular Aperture

The incident wave vector $\vec{k}$ is shown for the circular aperture in Figure 2-a. From the figure it is apparent that wave vector for the circular aperture has components of the form

$$k_x = k \cos\psi \tag{5}$$

$$k_y = -k \sin\psi \cos\zeta \tag{6}$$

$$k_z = -k \sin\psi \sin\zeta \quad . \tag{7}$$

The focusing function can be determined by considering the cross-sectional view of the aperture shown in Figure 2-b. Focusing requires that the effective propagation paths, and hence the phase, from every point in the aperture to the point $z = f, \rho' = o$ be the same. This requires that

$$r + \delta = b \text{ (constant)} \tag{8}$$

where

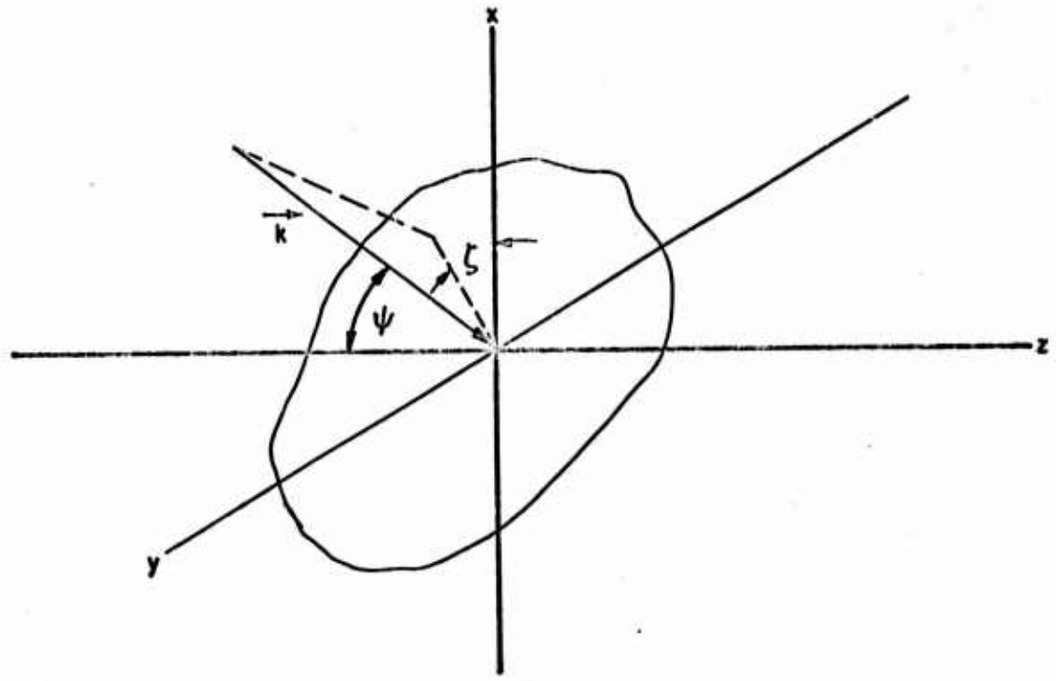

FIG. 2 -a INCIDENT WAVE VECTOR FOR A CIRCULAR APERTURE

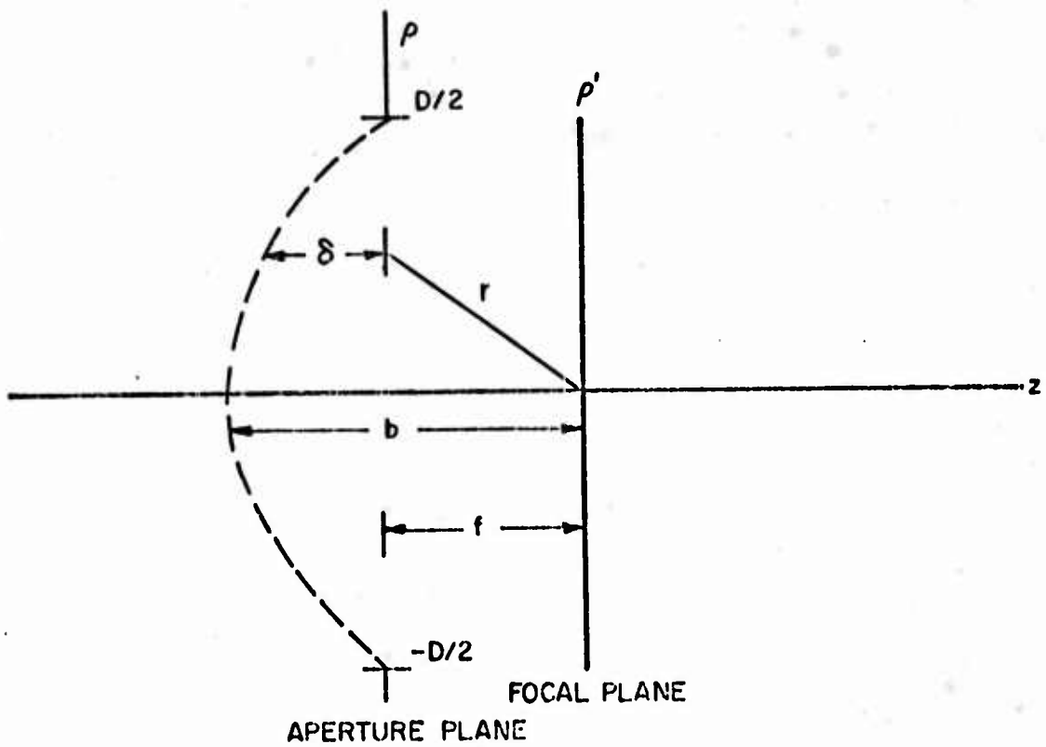

FIG. 2 -b PARAMETERS USED IN DERIVING THE FOCUSING FUNCTION δ

$$b = \left[\left(\frac{D}{2} \right)^2 + f^2 \right]^{\frac{1}{2}} \tag{9}$$

and

$$r = \left[\rho^2 + f^2 \right]^{\frac{1}{2}} . \tag{10}$$

The focusing function is symmetric in the variable ϕ, and can be found from Equation (8);

$$\delta(\rho) = \left[\left(\frac{D}{2} \right)^2 + f^2 \right]^{\frac{1}{2}} - \left[\rho^2 + f^2 \right]^{\frac{1}{2}} . \tag{11}$$

Equation (11) does not represent any particular structure, and in fact, when one applies Equation (11) to a particular case care must be taken in defining f and D.

The general definition of the geometric parameters of the circular aperture are given in Figure 3. Under the coordinate transformations,

$$z = z \tag{12}$$

$$x = \rho \cos \phi \tag{13}$$

$$y = \rho \sin \phi , \tag{14}$$

the form of the incident wave, accounting for focusing, becomes

$$U_S = E_o \, e^{ik[z \cos \psi - \rho \sin \psi \cos (\phi - \zeta) + \delta(\rho)]} . \tag{15}$$

The normal component of del operating on U_S is found by taking

$$\nabla U_S \cdot \hat{n} = \left[\frac{\partial U_S}{\partial \rho} \hat{\rho} + \frac{1}{\rho} \frac{\partial U_S}{\partial \phi} \hat{\phi} + \frac{\partial U_S}{\partial z} \hat{k} \right] \cdot \hat{n} \tag{16}$$

where

$$\hat{\rho} \cdot \hat{n} = 0, \; \hat{\phi} \cdot \hat{n} = 0, \; \hat{k} \cdot \hat{n} = -1 . \tag{17}$$

If the aperture plane is defined to be the plane at z = 0, then

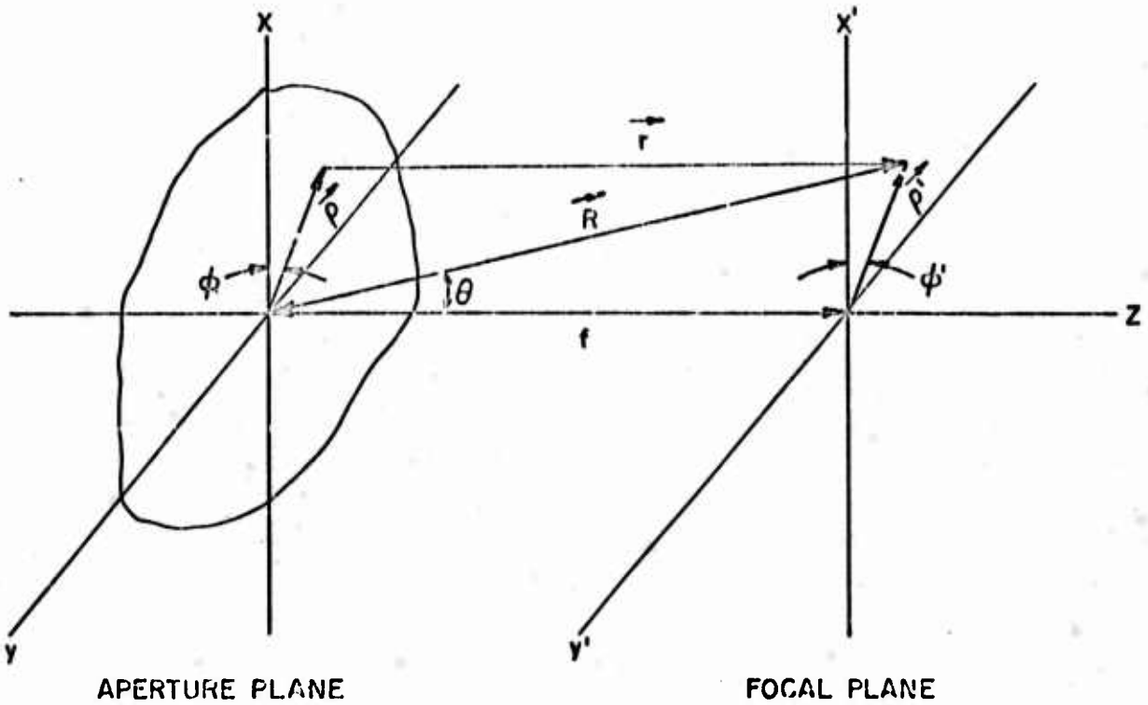

FIG. 3 - DEFINITION OF PARAMETERS FOR THE CIRCULAR APERTURE

$$\nabla U_S \cdot \hat{n} = -ik \cos\psi \, E_o \, e^{ik[-\rho \sin\psi \cos(\phi - \zeta) + \delta(\rho)]} \quad . \qquad (18)$$

Substitution into Equation (4) yields the field due to a circular aperture of diameter D;

$$U_P = \frac{-ik}{4\pi} E_o \int_{\rho=0}^{D/2} \int_{\phi=0}^{2\pi} \frac{F(\rho,\phi)}{r(\rho,\phi)} [\cos\psi + \cos(\hat{n}, \hat{r})] \, \rho \, d\rho \, d\phi \qquad (19)$$

where

$$F(\rho,\phi) = \exp[ik(r(\rho,\phi) - \rho \sin\psi \cos(\phi - \zeta) + \delta(\rho))] \qquad (20)$$

$$\cos(\hat{n}, \hat{r}) = \frac{f}{r(\rho,\phi)} \quad . \qquad (21)$$

It is desired to determine the field structure in the focal plane, defined as the plane perpendicular to the z axis through the point z = f. Hence, from Figure 3, the position vector r has the form,

$$r(\rho,\phi) = \left[f^2 + \rho^2 + \rho'^2 - 2\rho\rho' \cos(\phi - \phi')\right]^{\frac{1}{2}} \quad , \qquad (22)$$

and since

$$\rho' = f \tan\theta \qquad (23)$$

one can write

$$r(\rho,\phi) = \left[\frac{f^2}{\cos^2\theta} + \rho^2 - 2\rho f \tan\theta \cos(\phi - \phi')\right]^{\frac{1}{2}} \quad . \qquad (24)$$

Equation (19), with Equations (20), (21), and (24), represents the best expression for the focal plane field structure under the limitations of a scalar approach. The integral cannot be solved in closed form, but requires a numerical computer solution.

In an effort to simplify Equation (19) in order to gain physical insight into the problem, some further approximations can be made. Rewriting Equation (24) in the form

$$r(\rho,\phi) = \left(\frac{f^2}{\cos^2\theta} + \rho^2\right)^{\frac{1}{2}}\left[1 - \frac{2\rho f \tan\theta \cos(\phi-\phi')}{\frac{f^2}{\cos^2\theta} + \rho^2}\right]^{\frac{1}{2}}, \quad (25)$$

and considering only small θ, one can approximate the radical by the first two terms in the binomial expansion;

$$r(\rho,\phi) \approx \left(\frac{f^2}{\cos^2\theta} + \rho^2\right)^{\frac{1}{2}}\left[1 - \frac{\rho f \tan\theta \cos(\phi-\phi')}{\frac{f^2}{\cos^2\theta} + \rho^2}\right] . \quad (26)$$

This approximation will be used in the phase term $\left(F(\rho,\phi)\right)$ of Equation (19). The amplitude terms $\left(\text{terms other than } F(\rho,\phi)\right)$ in Equation (19) can be approximated by

$$r(\rho,\phi) \approx r(\rho) = (f^2 + \rho^2)^{\frac{1}{2}} \quad (27)$$

since they are slowly varying functions of θ. These approximations result in an integrand which is a separable function of ρ and ϕ, and Equation (19) takes the form

$$U_P \approx -\frac{ikE_o}{4\pi}\int_0^{D/2} \frac{F(\rho)\, e^{ik\left[a(\rho)+\delta(\rho)\right]}}{\left(f^2+\rho^2\right)^{\frac{1}{2}}}\left[\cos\psi + \frac{f}{\left(f^2+\rho^2\right)^{\frac{1}{2}}}\right]\rho d\rho , \quad (28)$$

with

$$F(\rho) = \int_0^{2\pi} \exp\left[-ik\left(\rho\sin\psi\cos(\phi-\zeta) + \frac{\rho f\tan\theta\cos(\phi-\phi')}{\left(\frac{f^2}{\cos^2\theta}+\rho^2\right)^{\frac{1}{2}}}\right)\right] d\phi \quad (29)$$

and

$$a(\rho) = \left(\frac{f^2}{\cos^2\theta} + \rho^2\right)^{\frac{1}{2}} . \qquad (30)$$

Equation (29) can be solved, and the solution is the zero order Bessel function,

$$F(\rho) = 2\pi J_o\left(k\,\eta(\rho)\right) \qquad (31)$$

where

$$\eta(\rho) = \left[\rho^2 \sin^2\psi + \frac{\rho^2 f^2 \tan^2\theta}{\frac{f^2}{\cos^2\theta} + \rho^2} + \frac{2\rho^2 f \tan\theta \sin\psi \cos(\zeta - \phi')}{\left(\frac{f^2}{\cos^2\theta} + \rho^2\right)^{\frac{1}{2}}}\right]^{\frac{1}{2}} . \qquad (32)$$

The resulting expression for the field in the focal plane is,

$$U_P \approx -\frac{ik}{2} E_o \int_0^{D/2} \frac{e^{ik\left[\left(\frac{f^2}{\cos^2\theta} + \rho^2\right)^{\frac{1}{2}} + \delta(\rho)\right]}}{\left(f^2 + \rho^2\right)^{\frac{1}{2}}} J_o\left(k\eta(\rho)\right)\left[\cos\psi + \frac{f}{\left(f^2 + \rho^2\right)^{\frac{1}{2}}}\right]\rho d\rho . \qquad (33)$$

This integration still requires a numerical computer solution. However, depending on the computer capability, the integration over a single variable may prove to be a valuable simplification.

2.2 Solution of Equation (4) for a Rectangular Aperture

The geometry for the rectangular aperture is shown in Figure 4-a. The incident wave vector, $\vec{k}$, is defined in Figure 4-b. By an anlysis similar to that for the circular aperture, one can show that the field in the focal plane of a rectangular aperture with sides a and b is given by,

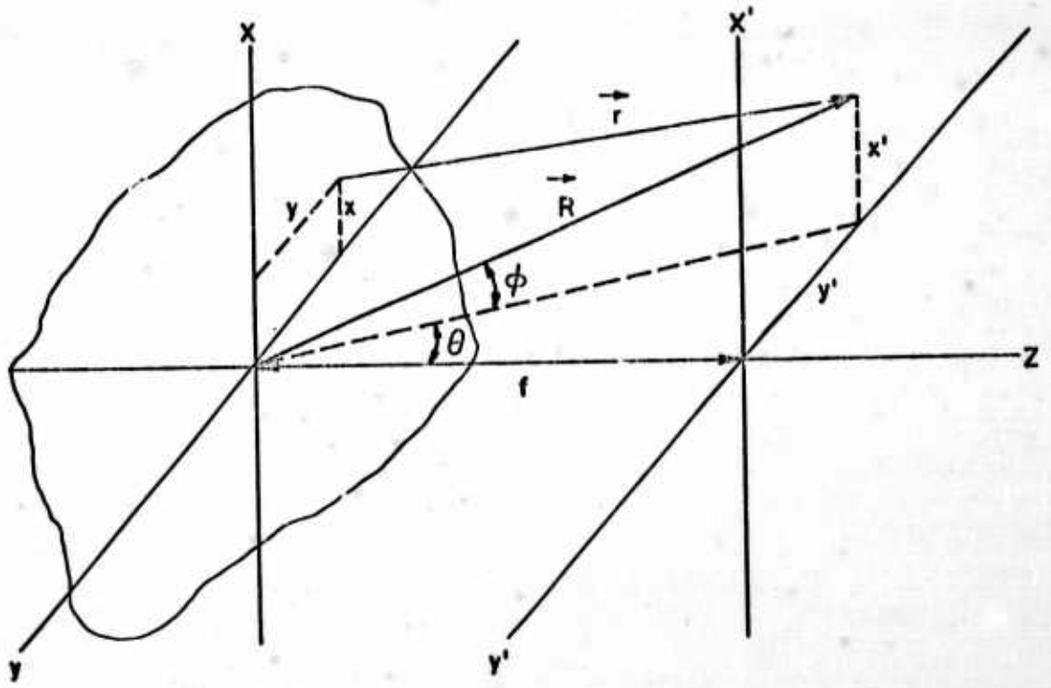

FIG. 4 -a DEFINITION OF PARAMETERS FOR THE RECTANGULAR APERTURE

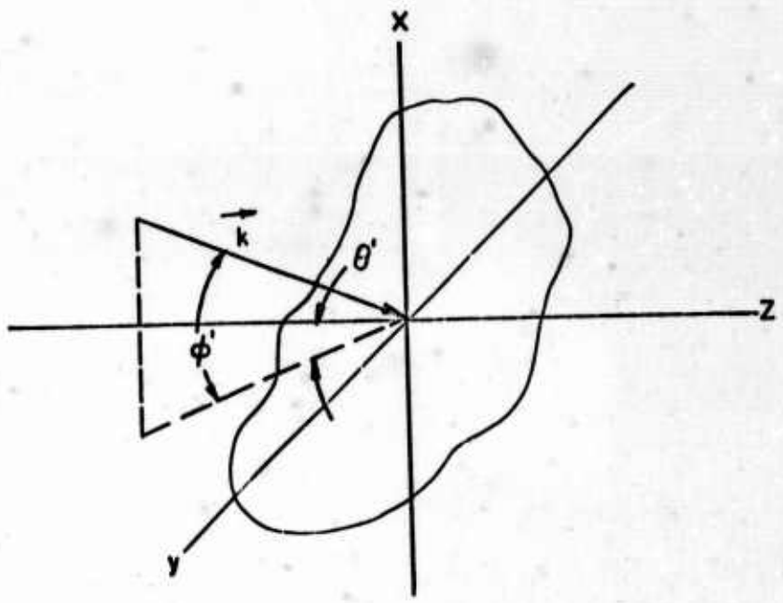

FIG. 4 -b DEFINITION OF INCIDENT WAVE VECTOR

$$U_P = -\frac{ik}{4\pi} E_o \int_{-a/2}^{a/2} \int_{-b/2}^{b/2} \frac{F(x,y)}{\left[f^2 + x^2 + y^2\right]^{\frac{1}{2}}} \left[\cos\phi' \cos\theta' + \frac{f}{\left[f^2 + x^2 + y^2\right]^{\frac{1}{2}}}\right] dxdy \,, \tag{34}$$

where

$$F(x,y) = \exp\left[ik\left(r(x,y) - x \sin\phi' - y \cos\phi' \sin\theta' + \delta(x,y)\right)\right] . \tag{35}$$

For this geometry, the position vector and focusing function are given by,

$$r(x,y) = \left[\frac{f^2}{\cos^2\phi \cos^2\theta} + x^2 + y^2 - 2f\left(x \frac{\tan\phi}{\cos\theta} + y \tan\theta\right)\right]^{\frac{1}{2}} \tag{36}$$

$$\delta(x,y) = \left[\frac{a^2 + b^2}{4} + f^2\right]^{\frac{1}{2}} - \left[x^2 + y^2 + f^2\right]^{\frac{1}{2}} \tag{37}$$

Because there is only slight interest in focused rectangular apertures, this analysis has not been pursued further.

2.3 Two Dimensional Diffraction by an Infinite Slit

The analysis of the two dimensional problem requires some modification of the Fresnel-Kirchhoff equation (1). Assume a volume V which is much larger in length than in any radial dimension. Hence, cylindrical coordinates will be used to describe V. The pertinent geometry is shown in Figure 5. Assume two functions, U and v, which are solutions of the wave equation and hence obey Green's second identity;

$$\nabla^2(U,v) + k^2(U,v) = 0 \tag{38}$$

$$\oint_S \left[v \nabla U - U \nabla v\right] \cdot \hat{n} dS = 0 \,. \tag{39}$$

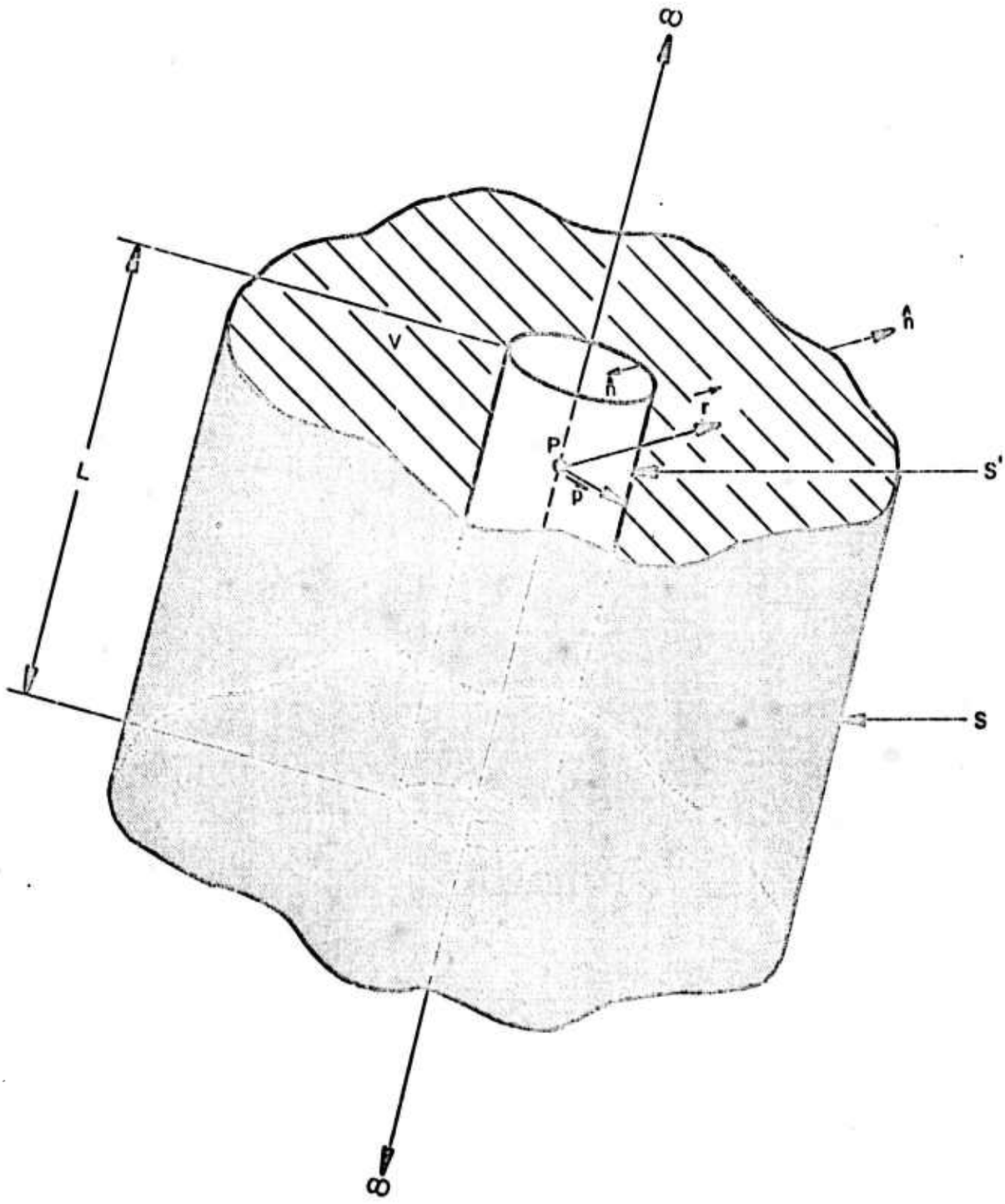

FIG. 5-GEOMETRY FOR TWO DIMENSIONAL DIFFRACTION

In the cylindrical coordinates, the choice for v which satisfies the wave equation is

$$v = i\pi H_o^{(1)}(kr) \quad , \tag{40}$$

where $H_o^{(1)}$ is the zero order Hankel function of the first kind. We will be interested in the asymptotic forms,

$$i\pi H_o^{(1)}(kr) \rightarrow \begin{cases} -2\ln(kr), & r \rightarrow 0 \\ i\sqrt{\frac{2\pi}{kr}} \; e^{i(kr - \pi/4)}, & r \rightarrow \infty \end{cases} . \tag{41}$$

To evaluate the disturbance along a line through P, of length L, both asymptotic regions must be considered. Therefore, divide the volume V with a sub-volume defined by the surface S'. Equation (39) then becomes

$$\oint_S [v \nabla U_S - U_S \nabla v] \cdot \hat{n} dS = - \oint_{S'} [v \nabla U_{S'} - U_{S'} \nabla v] \cdot \hat{n} dS' \quad . \tag{42}$$

Let ρ be the radius of the cylinder with surface S', and as ρ becomes small

$$v = i\pi H_o^{(1)}(k\rho) \rightarrow -2\ln(k\rho) \quad . \tag{43}$$

The normal component of del operating on v results in

$$\nabla v \cdot \hat{n} = \frac{\partial v}{\partial n} = -\frac{\partial v}{\partial \rho} \quad , \tag{44}$$

where the minus sign results from the direction of $\hat{n}$ being out of the volume V as shown in Figure 5. Applying the Hankel identities to Equation (44), along with the small argument asymptotic approximation yields

$$-\frac{\partial v}{\partial \rho} = i\pi k H_1^{(1)}(k\rho) \to \frac{2}{\rho} \quad . \tag{45}$$

Substituting Equations (43) and (45) into the right hand side of Equation (42) (which is the integration over S' where the above approximations are valid) results in

$$-\oint_{S'} [v\nabla U_{S'} - U_{S'}\nabla v] \cdot \hat{n} dS' = \oint_{S'} [2 \ln(k\rho) \nabla U_{S'}] \cdot \hat{n} dS' + \oint_{S'} U_{S'}\left(\frac{2}{\rho}\right) dS' \quad . \tag{46}$$

In the limit as ρ becomes vanishingly small, Equation (46) yields only one term;

$$\lim_{\rho \to 0} \oint_{S'} U_{S'}\left(\frac{2}{\rho}\right) \rho d\phi \, dz \to 4\pi L U_{S'} \quad , \tag{47}$$

$$\lim_{\rho \to 0} \oint_{S'} [-2 \ln(k\rho) \nabla U_{S'}] \cdot \hat{n} \, \rho d\phi \, dz \to 0 \quad . \tag{48}$$

Therefore, Equation (42) becomes,

$$4\pi L U_P = \oint_S [v\nabla U_S - U_S \nabla v] \cdot \hat{n} dS \quad . \tag{49}$$

Over the surface S, the large argument approximation holds for v,

$$v = i\pi H_o^{(1)}(kr) \to i\sqrt{\frac{2\pi}{kr}} \, e^{i(kr - \pi/4)} \tag{50}$$

and

$$\nabla v \cdot \hat{n} = \frac{\partial v}{\partial r}(\hat{r} \cdot \hat{n}) = -i\pi k H_1^{(1)}(kr) \cos(\hat{r}, \hat{n}) \quad . \tag{51}$$

Considering the large argument asymptotic form of Equation (51),

$$\nabla v \cdot \hat{n} \rightarrow -ik \sqrt{\frac{2\pi}{kr}}\; e^{\,i(kr - 3\pi/4)} \cos(\hat{r}, \hat{n}) \quad . \tag{52}$$

Substitute Equations (50) and (52) into Equation (49) to show that,

$$4\pi L\, U_P = \oint_S i \sqrt{\frac{2\pi}{kr}}\; e^{\,i(kr - \pi/4)} [\nabla U_S \cdot \hat{n} - ikU_S \cos(\hat{r}, \hat{n})]\; r\, d\phi dz \quad . \tag{53}$$

Integration with respect to z causes the length (L) dependence to drop out of Equation (53). The two dimensional equivalent to the three dimensional Fresnel-Kirchhoff integral of Equation (1) is,

$$U_P = \frac{i}{4\pi} \oint \sqrt{\frac{2\pi}{kr}}\; e^{\,i(kr - \pi/4)} [\nabla U_S \cdot \hat{n} - ikU_S \cos(\hat{r}, \hat{n})]\; d\ell \quad , \tag{54}$$

where

$$r d\phi = d\ell \quad .$$

The line ℓ is the perimeter of a slice of the volume V containing the point P. As in the three dimensional case, we will assume that U_S and $\nabla U_S \cdot \hat{n}$ are zero everywhere on ℓ except in the aperture. This reduces the integral equation (54) to an integration over the aperture.

A cross-sectional view of the infinite slit is given in Figure 6. The incident wave will be of the form given in Equation (3), and this particular geometry results in

$$U_S = E_o\, e^{\,ik[y \cos\theta' - x \sin\theta' + \delta(x)]} \quad . \tag{55}$$

The focusing function, $\delta(x)$, must produce a spherical phase distribution whose radius of curvature is centered at the point $y = f$, $x' = 0$. Such a function is given by,

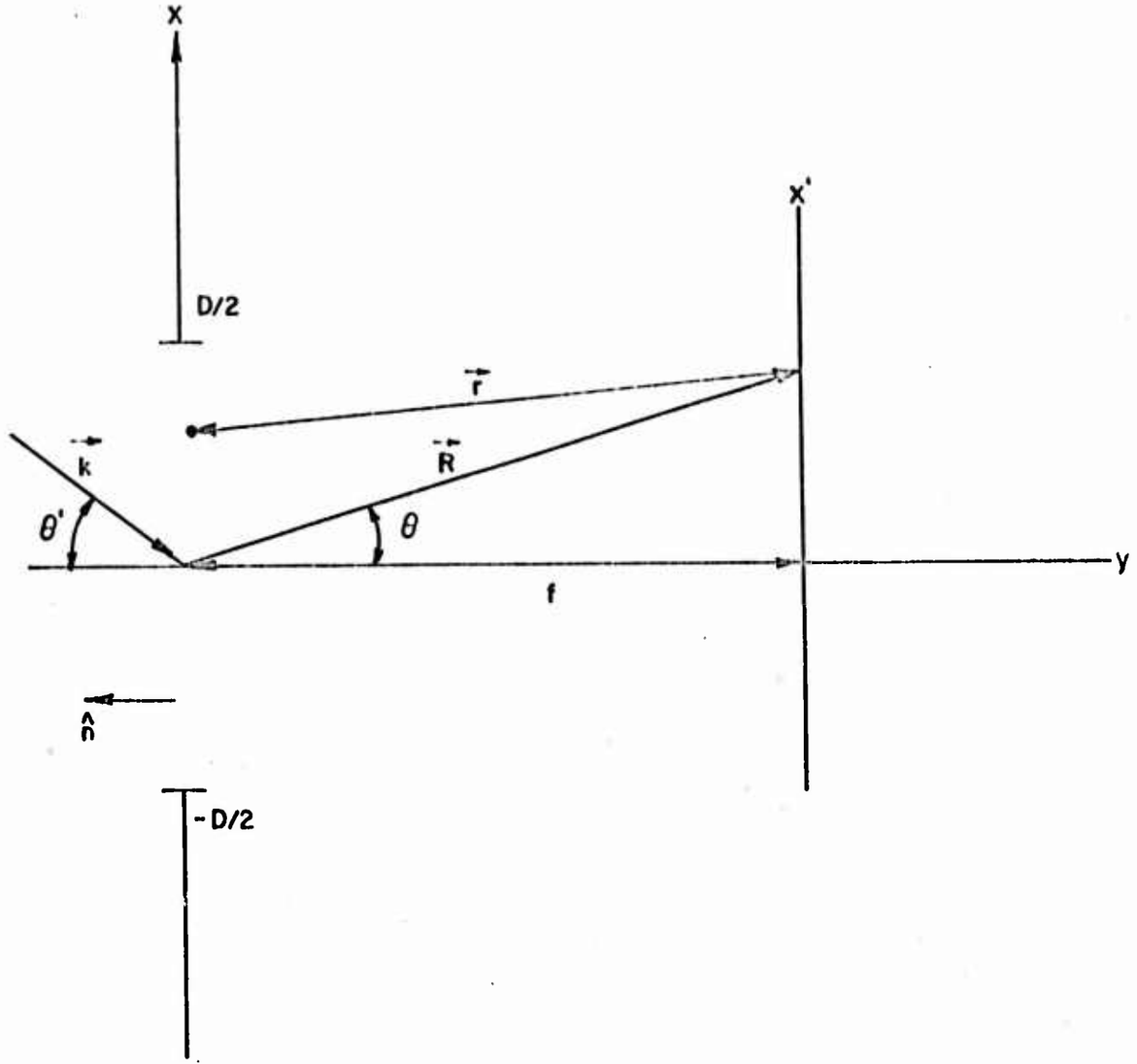

FIG. 6 - DEFINITION OF THE PARAMETERS FOR THE INFINITE SLIT (TWO DIMENSIONAL DIFFRACTION PROBLEM)

$$\delta(x) = \left[\left(\frac{D}{2}\right)^2 + f^2 \right]^{\frac{1}{2}} - \left[x^2 + f^2 \right]^{\frac{1}{2}} \qquad (56)$$

The normal gradient of the incident wave is found by,

$$\nabla U_S \cdot \hat{n} = \left[\frac{\partial U_S}{\partial x} \hat{i} + \frac{\partial U_S}{\partial y} \hat{j} \right] \cdot \hat{n} \ , \qquad (57)$$

where

$$\hat{i} \cdot \hat{n} = 0, \quad \hat{j} \cdot \hat{n} = -1 \ ,$$

and therefore,

$$\nabla U_S \cdot \hat{n} = - ik \cos 0' \, E_o \, e^{ik[y \cos 0' - x \sin 0' + \delta(x)]} \ . \qquad (58)$$

Taking the aperture in the plane defined by $y = 0$ reduces Equation (54) to the form,

$$U_P = \frac{1}{2} \sqrt{\frac{k E_o^2}{2\pi}} \int_{-D/2}^{D/2} \frac{F(x)}{[r(x)]^{\frac{1}{2}}} \left[\cos 0' + \cos (\hat{n}, \hat{r}) \right] dx \qquad (59)$$

where

$$F(x) = \exp \left\{ ik \left[r(x) - x \sin 0' + \delta(x) \right] - i \frac{\pi}{4} \right\} \ . \qquad (60)$$

The magnitude of the position vector, $\vec{r}$, is given by

$$[r(x)]^2 = f^2 + (x - x')^2 \ , \qquad (61)$$

which can be expanded to give

$$r(x) = \left[\frac{f^2}{\cos^2 \theta} + x^2 - 2 x f \tan 0 \right]^{\frac{1}{2}} \ . \qquad (62)$$

The direction cosine is given by,

$$\cos (\hat{n}, \hat{r}) = \frac{f}{r(x)} \ . \qquad (63)$$

A more convenient form of Equation (59) can be generated by normalizing with respect to wavelength;

$$U_P = \frac{E_o}{2} \int_{-D/2\lambda}^{D/2\lambda} \frac{c}{\left[\frac{r(x)}{\lambda}\right]^{\frac{1}{2}}} e^{i\left[2\pi\left(\frac{r(x)}{\lambda} - \frac{x}{\lambda}\sin\theta' + \frac{\delta(x)}{\lambda}\right) - \frac{\pi}{4}\right]} \left[\cos\theta' + \frac{\frac{f}{\lambda}}{\frac{r(x)}{\lambda}}\right] d\left(\frac{x}{\lambda}\right) , \tag{64}$$

where

$$\frac{r(x)}{\lambda} = \left[\frac{1}{\cos^2\theta}\left(\frac{f}{\lambda}\right)^2 + \left(\frac{x}{\lambda}\right)^2 - 2\left(\frac{x}{\lambda}\right)\left(\frac{f}{\lambda}\right)\tan\theta\right]^{\frac{1}{2}} \tag{65}$$

$$\frac{\delta(x)}{\lambda} = \left[\left(\frac{D}{2\lambda}\right)^2 + \left(\frac{f}{\lambda}\right)^2\right]^{\frac{1}{2}} - \left[\left(\frac{x}{\lambda}\right)^2 + \left(\frac{f}{\lambda}\right)^2\right]^{\frac{1}{2}} \tag{66}$$

Equation (64) represents the complex field structure of an infinite slit focused in its near field. The integral cannot be solved in closed form. Since it must be applied for each angle of arrival (θ') and solved for a high density of values of diffraction angle (θ), a substantial computer effort is involved. For this reason, a perturbation technique has been investigated. Expand Equation (64) in a Maclaurin series in the variable θ',

$$U_P(\theta') = U_P(\theta' = 0) + \sum_{n=0}^{k} \left[\frac{\partial^n U_P}{\partial \theta'^n}\right]_{\theta' = 0} \frac{\theta'^n}{n!} . \tag{67}$$

The first three perturbation terms are,

$$U_P(\theta' = 0) = \frac{E_o}{2} \int_{-D/2\lambda}^{D/2\lambda} \frac{c}{\left[\frac{r(x)}{\lambda}\right]^{\frac{1}{2}}} e^{i\left[2\pi\left(\frac{r(x)}{\lambda} + \frac{\delta(x)}{\lambda}\right) - \frac{\pi}{4}\right]} \left[1 + \frac{\frac{f}{\lambda}}{\frac{r(x)}{\lambda}}\right] d\left(\frac{x}{\lambda}\right) , \tag{68}$$

$$\left[\frac{\partial U_P}{\partial \theta'}\right]_{\theta'=0} \theta' = -i\pi E_o \theta' \int_{-D/2\lambda}^{D/2\lambda} \left(\frac{x}{\lambda}\right) \frac{e^{i\left[2\pi\left(\frac{r(x)}{\lambda}+\frac{\delta(x)}{\lambda}\right)-\frac{\pi}{4}\right]}}{\left[\frac{r(x)}{\lambda}\right]^{\frac{1}{2}}} \left[1+\frac{\frac{f}{\lambda}}{\frac{r(x)}{\lambda}}\right] d\left(\frac{x}{\lambda}\right) , \tag{69}$$

and

$$\left[\frac{\partial^2 U_P}{\partial \theta'^2}\right]_{\theta'=0} \frac{\theta'^2}{2!} = -\frac{E_o}{4} \theta'^2 \int_{-D/2\lambda}^{D/2\lambda} \frac{e^{i\left[2\pi\left(\frac{r(x)}{\lambda}+\frac{\delta(x)}{\lambda}\right)-\frac{\pi}{4}\right]}}{\left[\frac{r(x)}{\lambda}\right]^{\frac{1}{2}}} \left[4\pi^2\left(\frac{x}{\lambda}\right)^2\left(1+\frac{\frac{f}{\lambda}}{\frac{r(x)}{\lambda}}\right)+1\right] d\left(\frac{x}{\lambda}\right) . \tag{70}$$

This approach offers the simplification that integrals are solved once for some range of diffraction angle θ. The treatment of off axis waves is then reduced to the algebraic operation of Equation (67). This advantage assumes that Equation (67) converges for some reasonable number k. Since the various ordered derivatives are directly multiplied by θ'^n, this condition is easier to satisfy for small θ'. Some insight into the rate of convergence can be gained by considering Equation (67) at the particular value of diffraction angle, $\theta = 0$. At this value of θ the integrands of the various perturbation orders have the same parity as the order number. With the symmetric limits of integration, we only get a contribution from the even order perturbation terms. This yields the interesting result that, in order to have some correction at all values of θ, $k \geq 2$. Another result of using $\theta = 0$ is that the integrands are nonoscillatory functions, and hence solution by planimeter measurement is quite simple. This has been done, up to and including $k = 4$, for an $f/D = .25$ and $D/\lambda = 50$. In order to have an exact value for comparison to the perturbation approximation, Equation (64) has also been planimeter integrated.

At the value $\theta = 0$, the only contribution to this integral is from the cosine term:

$$U_p(\theta=0) = \text{const.} \int_{-D/2\lambda}^{D/2\lambda} \frac{\cos\left[2\pi \frac{x}{\lambda} \sin\theta'\right]}{\left[\left(\frac{f}{\lambda}\right)^2 + \left(\frac{x}{\lambda}\right)^2\right]^{\frac{1}{2}}} \left[\cos\theta' + \frac{\frac{f}{\lambda}}{\left[\left(\frac{f}{\lambda}\right)^2 + \left(\frac{x}{\lambda}\right)^2\right]^{\frac{1}{2}}}\right] d\left(\frac{x}{\lambda}\right) . \tag{71}$$

Although this is an oscillating integrand, and requires more calculated points to define the curve, for small θ' it oscillates very slowly. Plots of the integrand for some small values of θ' are given in Figure 7. $|U_p|^2$ from Equation (71) has been compared to the perturbation expansion of Equation (67), and the results are given in the following table:

$|U_p|^2 (\theta = 0)$

$\theta'(^\circ)$	Equation (71)	Equation (67), k = 2	Equation (67), k = 4
0	107.995	----	----
.1	105.808	105.812	105.820
.5	63.339	60.255 (.2 dB)	63.884 (.03 dB)
1.0	8.992	.013((28.2 dB)	12.717 (1.5 dB)
1.5	.211	172.865 (29.3 dB)	29.113 (21.4 dB)

The numbers in parentheses indicate the departure of the perturbation approximation from a solution of the exact expression. This shows that for k = 4, the perturbation application is limited to angles less than 1°. To apply Equation (67) with k = 4 requires a computer solution of five integral equations. In light of the limited range of θ' for which this would have application, it was decided to solve Equation (64) exactly for selected values of θ'.

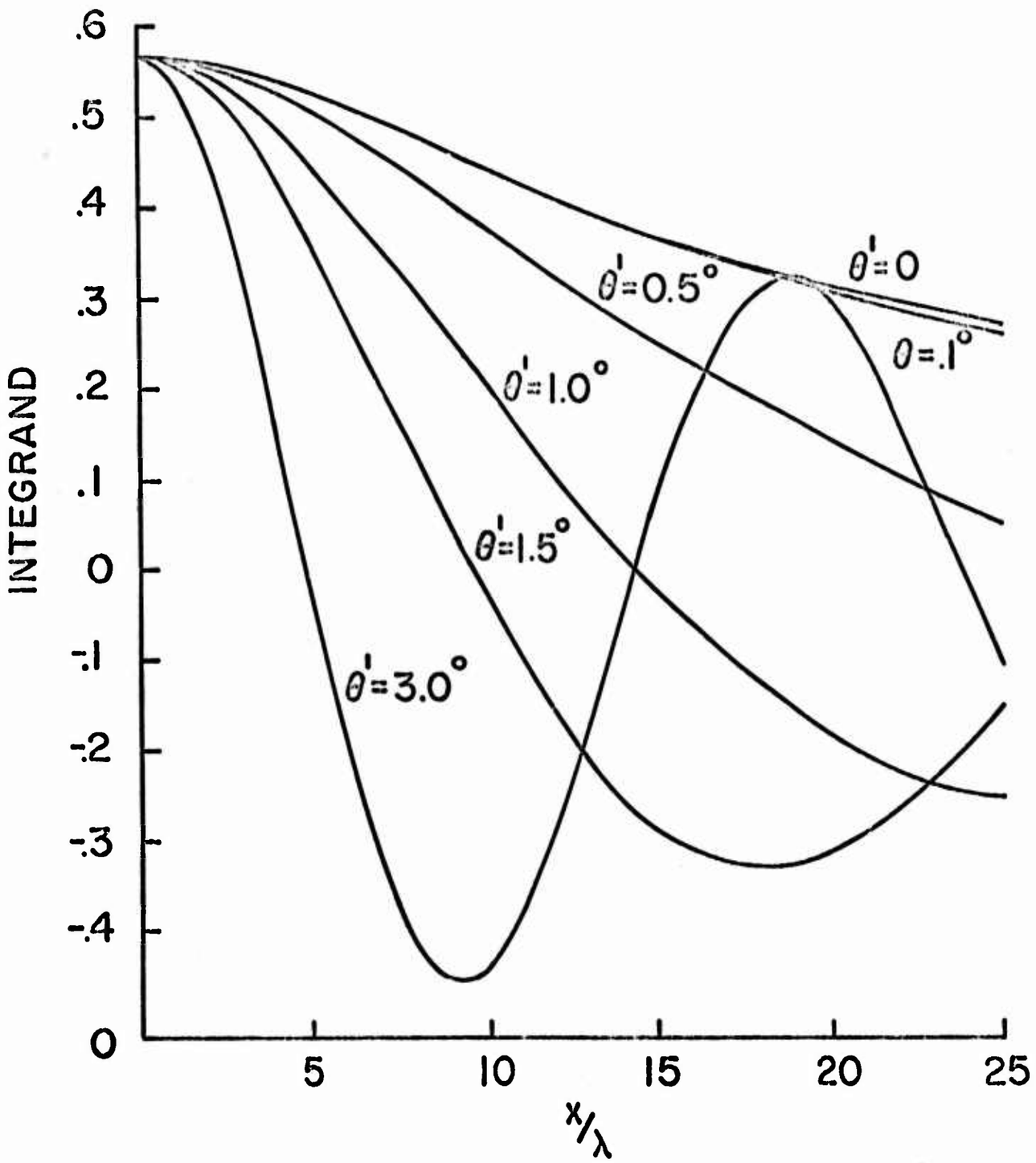

FIG. 7- INTEGRAND OF EQUATION (71) FOR SEVERAL VALUES OF ANGLE OF ARRIVAL.

Equation (64) has been expanded into the form,

$$U_p = A + i\,B \quad . \tag{72}$$

The distribution of power in the focal plane is given by,

$$\text{Power}\,(\theta)\,(\text{dB}) = 10\,\text{Log}_{10}\left|U_p(\theta)\right|^2 \quad , \tag{73}$$

and the phase angle is given by,

$$\text{Phase Angle}\,(\theta) = \tan^{-1}\frac{B(\theta)}{A(\theta)} \quad . \tag{74}$$

A computer program for the solution of Equations (73) and (74) is given as an Appendix to this report. Computations have been performed for diffraction angles ranging from -10° to $+10^\circ$. These were performed for the particular cases of $f/D = .25$, $D/\lambda = 50$, and $\theta' = 0^\circ$, 0.5°, 1.0°, 1.5°, 2.0°, 3.0°.

The solution of Equation (73) is given for normal incidence ($\theta' = 0$) in Figure 8. There is a significant difference between this pattern and the usually assumed Fraunhofer pattern. Within the range of θ for which computations have been performed, there is a spreading of the pattern and substantially higher sidelobe levels. Figure 8 includes a scale in λ/D in order to facilitate comparison of the new patterns to the Fraunhofer pattern. Interesting points of comparison are summarized in the following table:

	Fraunhofer Approximation	Equation (73)
3 dB point	$\theta = 0.56^\circ$	$\theta = 0.90^\circ$
1st null	$\theta = 1.15^\circ$	$\theta = 2.0^\circ$
1st sidelobe level	-13.48 dB	-7.4 dB
2nd null	$\theta = 2.3^\circ$	$\theta = 4.6^\circ$
2nd sidelobe level	-17.92 dB	-10.55 dB
3rd null	$\theta = 3.45^\circ$	$\theta = 7.25^\circ$
3rd sidelobe level	-20.84 dB	-12.70 dB
4th null	$\theta = 4.6^\circ$	$\theta = 9.8^\circ$

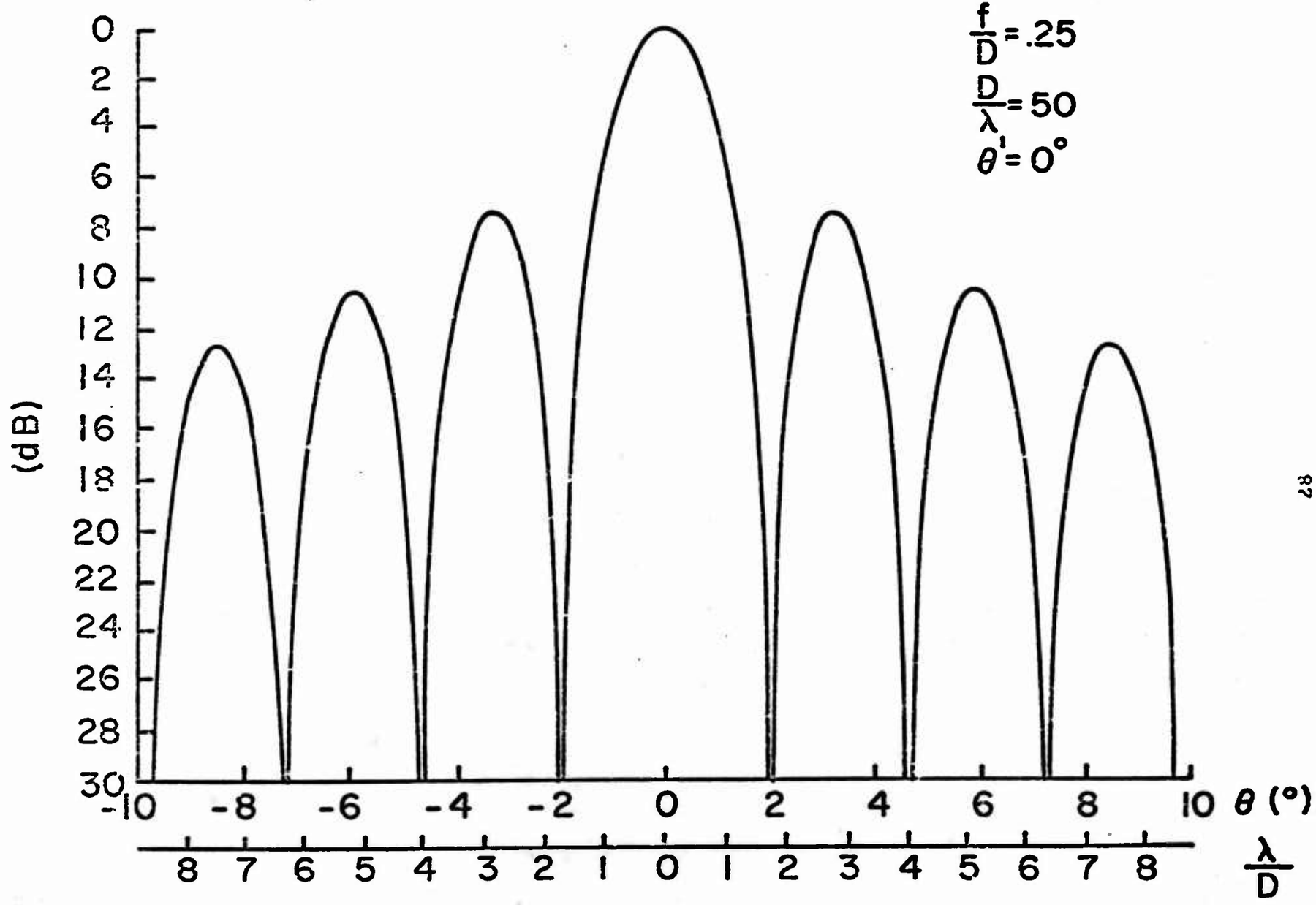

FIG.8 - THEORETICAL POWER PATTERN FOR NORMAL INCIDENCE

The phase distribution in the focal plane is given for this case in Figure 9. It is very similar to the phase behavior of the Fraunhofer pattern, with discontinuous steps of about π radians corresponding to the locations of nulls of the power pattern. The skirts on the leading and trailing edges of the phase curves are probably due to computational errors. The program was run in single precision. In the vicinity of power nulls, the functions A and B are very small numbers, and hence computational errors are more significant.

Very interesting comparisons can be made between this solution for the continuous aperture and previous results for an array of closely spaced elements. The continuous infinite slit would be related to the line array. Ricardi[7] has analyzed the case of a line array focused in its near field, with emphasis on determining the 3 dB spot size. Results corresponding to our situation ($f/D = .25$, $D/\lambda = 50$) are given by Hansen[8] and indicate a 0.4λ spot size for the array. This would correspond to a diffraction angle of $.92^\circ$, which is in excellent agreement with our angle of $.90^\circ$.

The power patterns for $\theta' = 0.5^\circ$, 1.0°, 1.5°, 2.0°, and 3.0° are given in Figures 10 through 14. Their associated phase distributions are given in Figures 15 through 19. Two interesting points can be noted from the patterns. There is a gross lack of symmetry not predicted by the Fraunhofer approximation. Also, the main beam is shifted by an angle larger than

---

7. Ricardi, L.J., Electromagnetic Theory and Antennas, (E.C. Jordan, ed.), "Near-Field Characteristics of a Linear Array", Proc. URSI Symp. Electromagnetic Theory and Antennas, Copenhagen, June 1962, Pergamon Press.

8. Hansen, R.C., Microwave Scanning Antennas, Vol. I, "Apertures", Academic Press, New York (1964), p. 44.

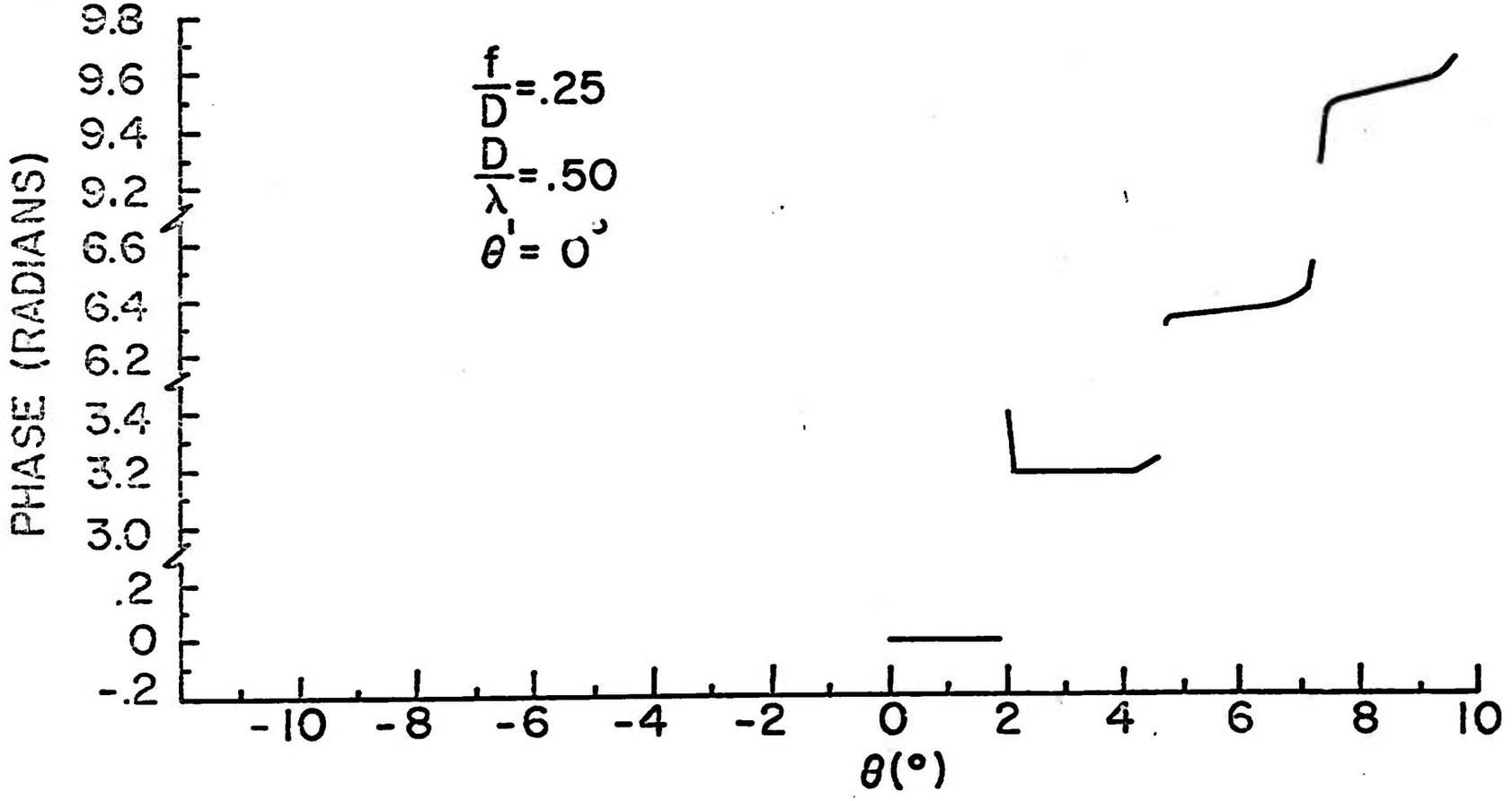

FIG. 9-THEORETICAL PHASE FOR NORMAL INCIDENCE

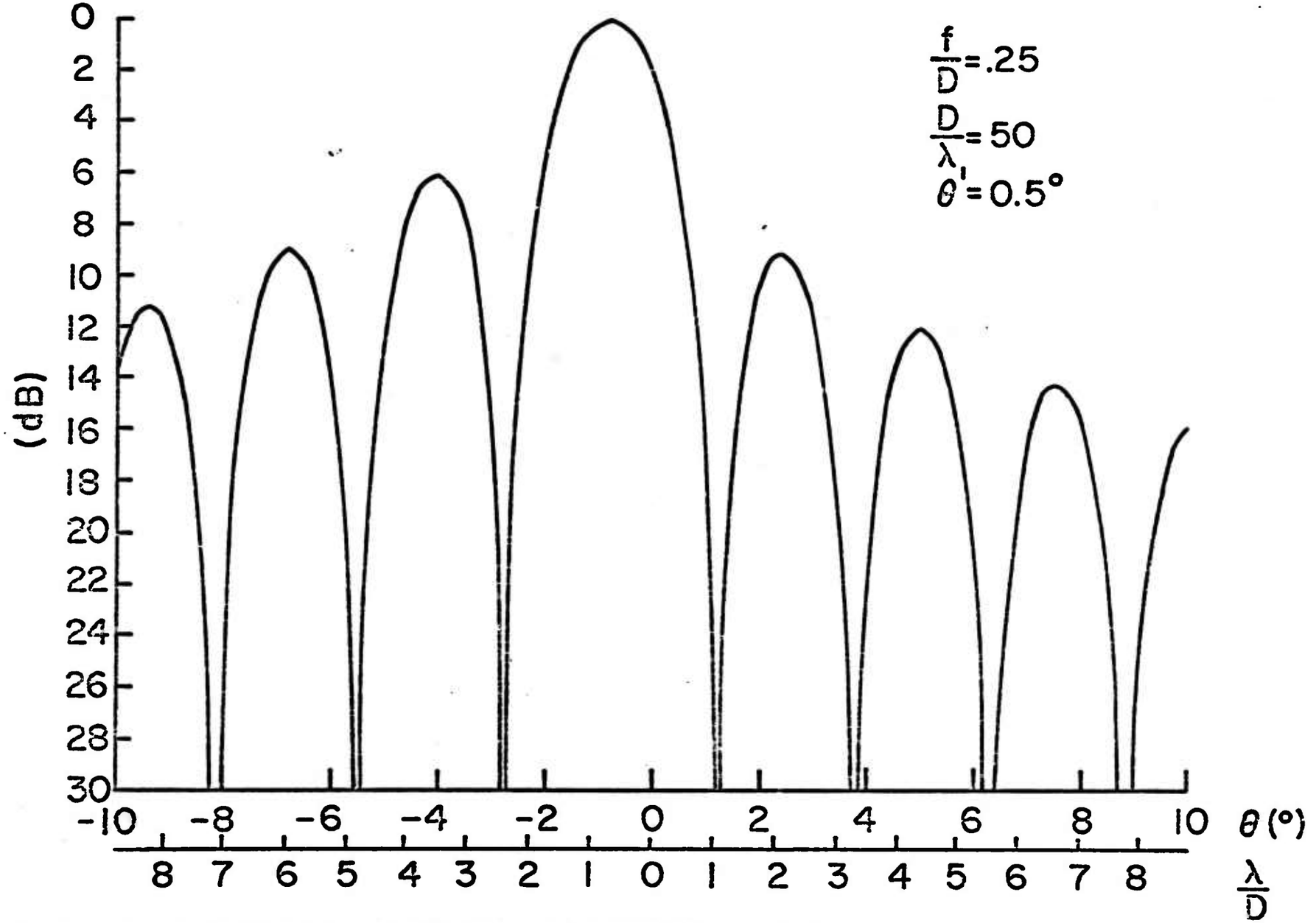

FIG.10-THEORETICAL POWER PATTERN FOR AN ANGLE OF ARRIVAL (0.5°)

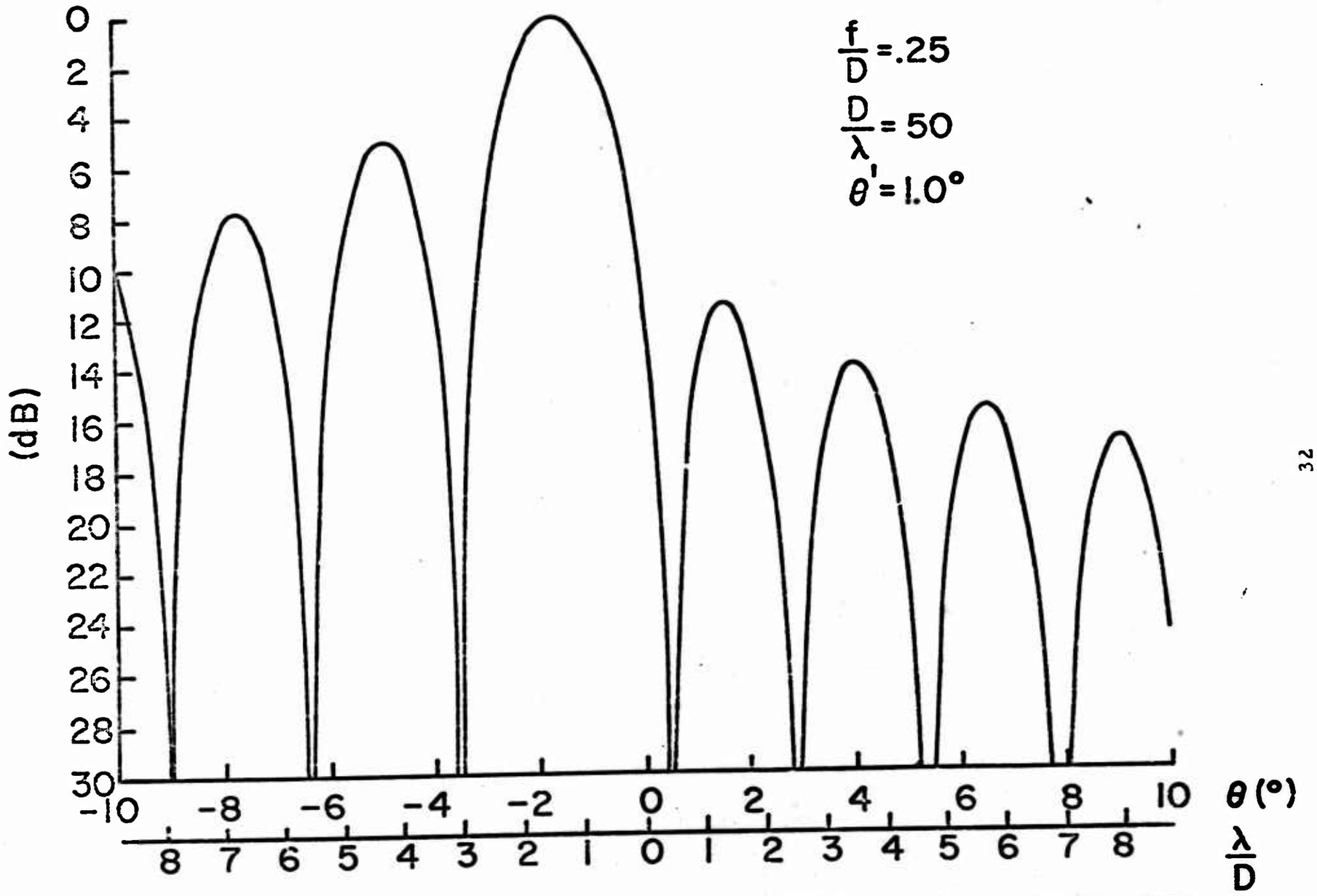

FIG.11 -THEORETICAL POWER PATTERN FOR AN ANGLE OF ARRIVAL (1.0°)

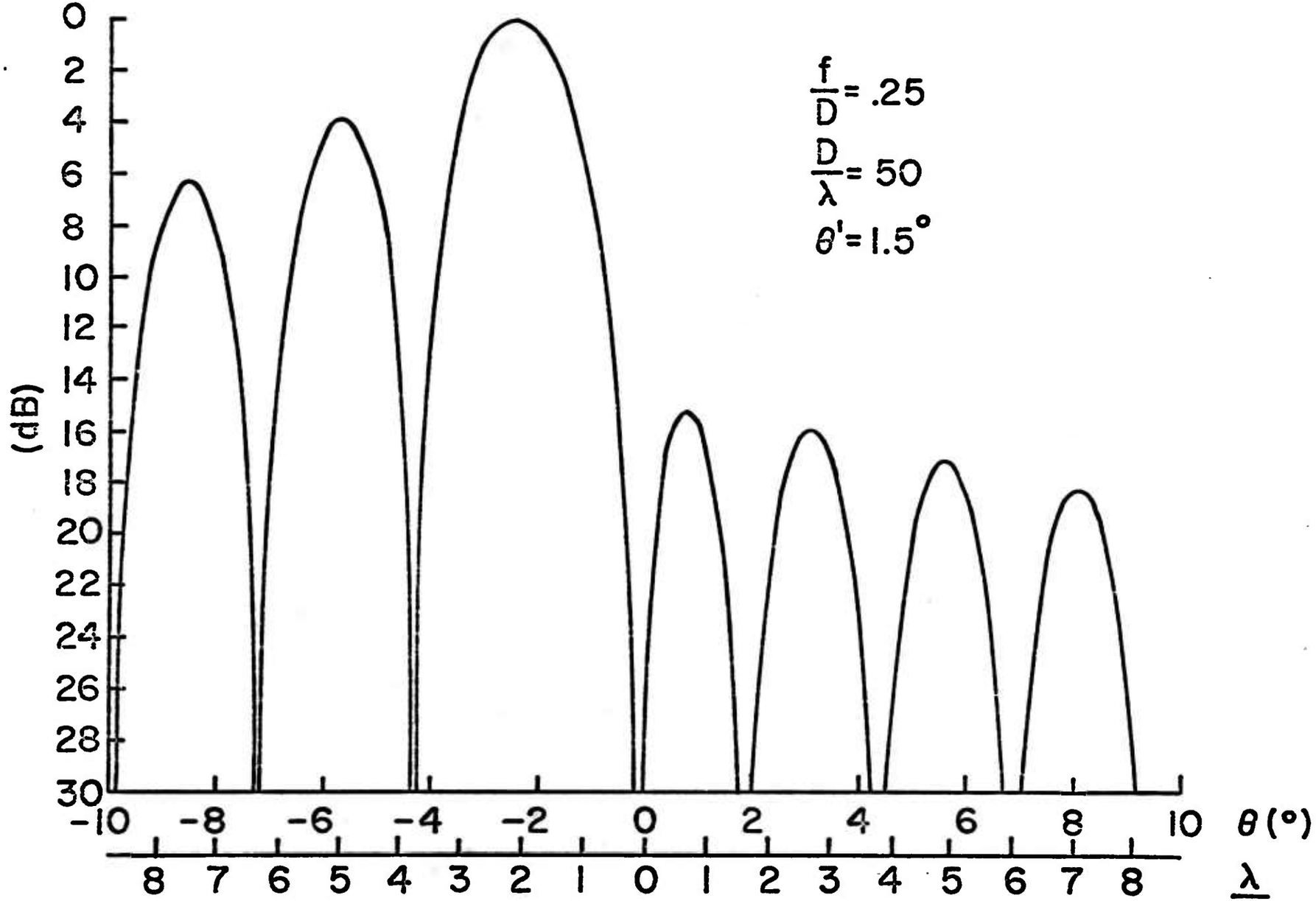

FIG.12-THEORETICAL POWER PATTERN FOR AN ANGLE OF ARRIVAL (1.5°)

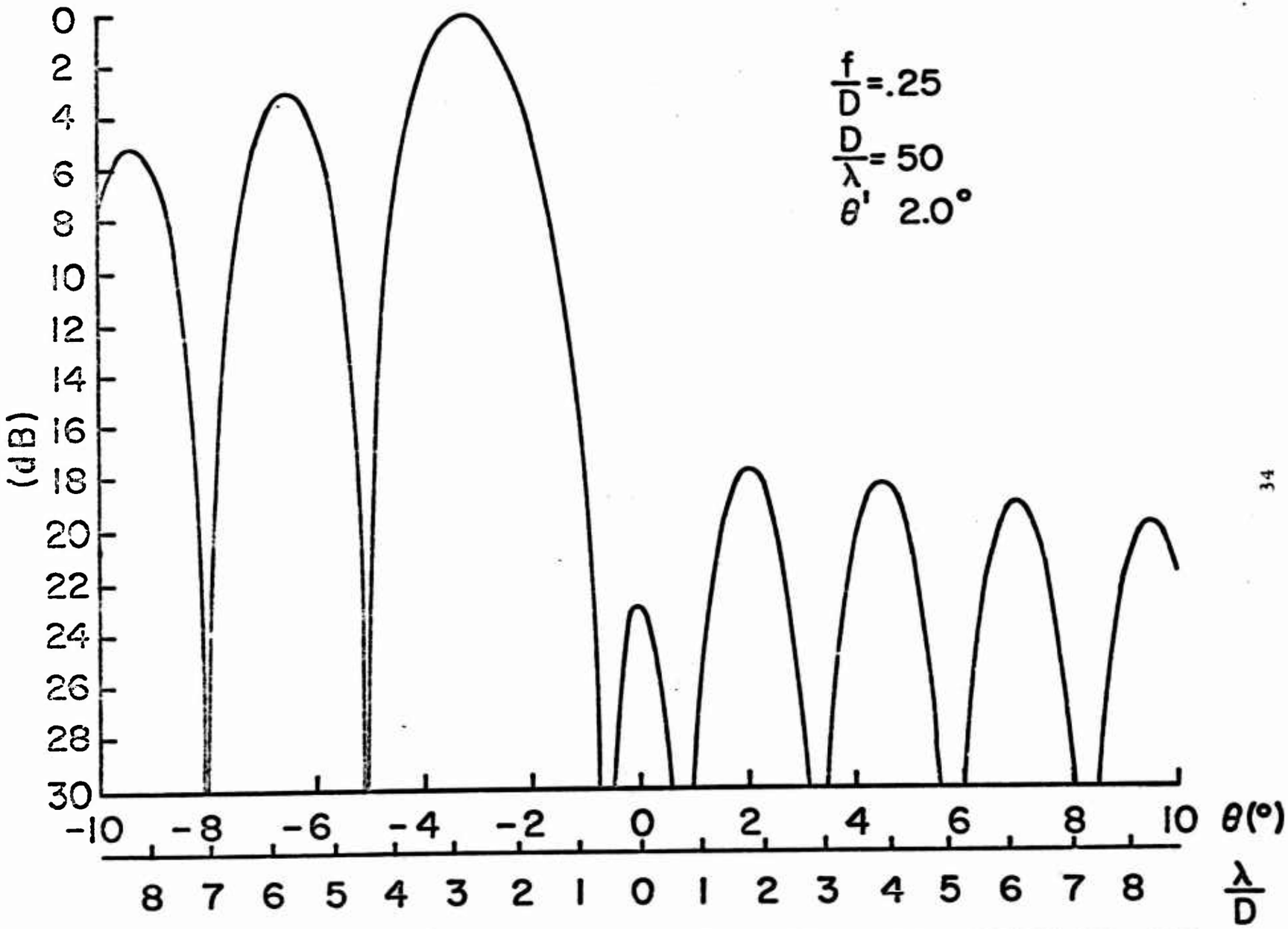

FIG.13-THEORETICAL POWER PATTERN FOR AN ANGLE OF ARRIVAL (2.0°)

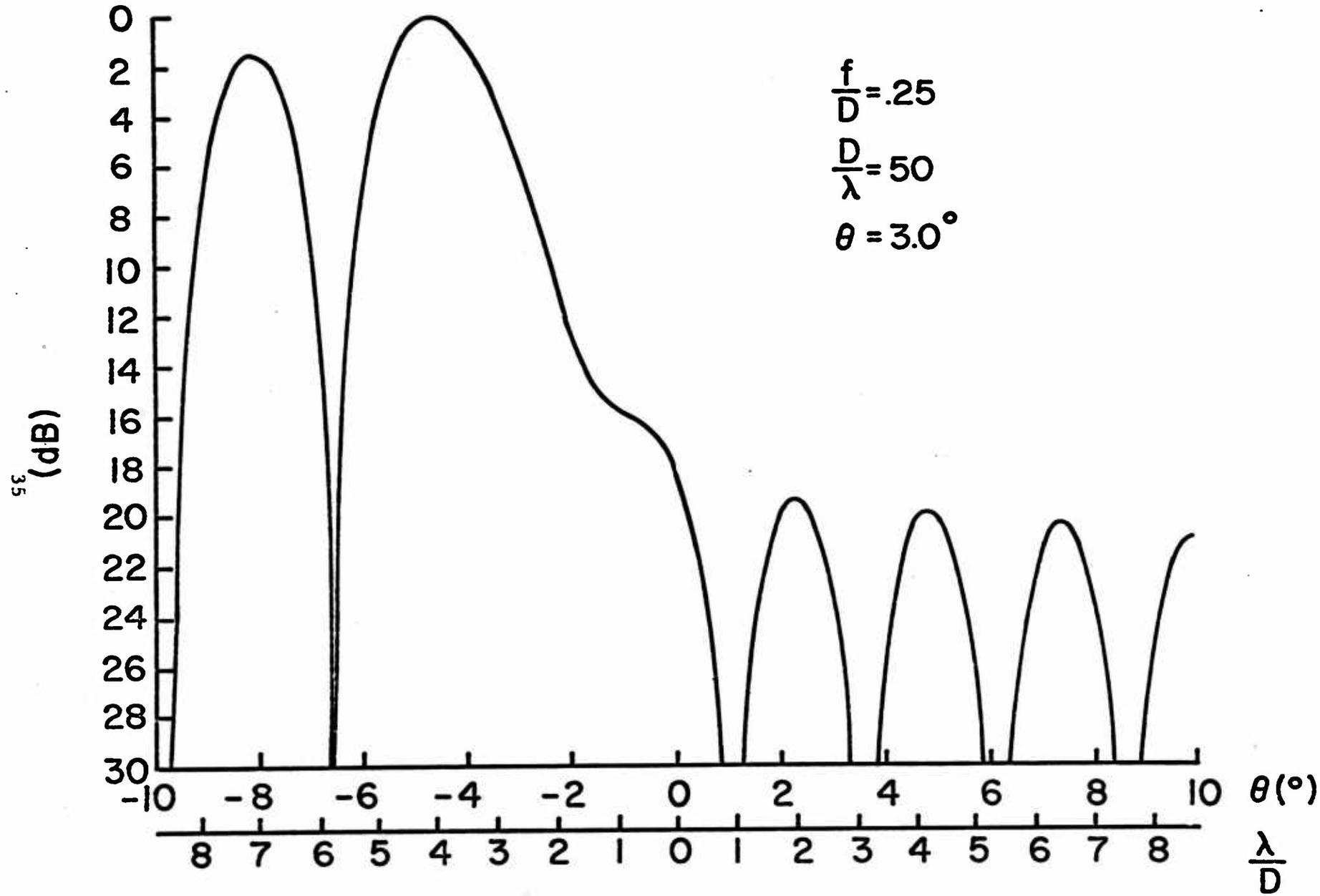

FIG.14-THEORETICAL POWER PATTERN FOR AN ANGLE OF ARRIVAL (3.0°)

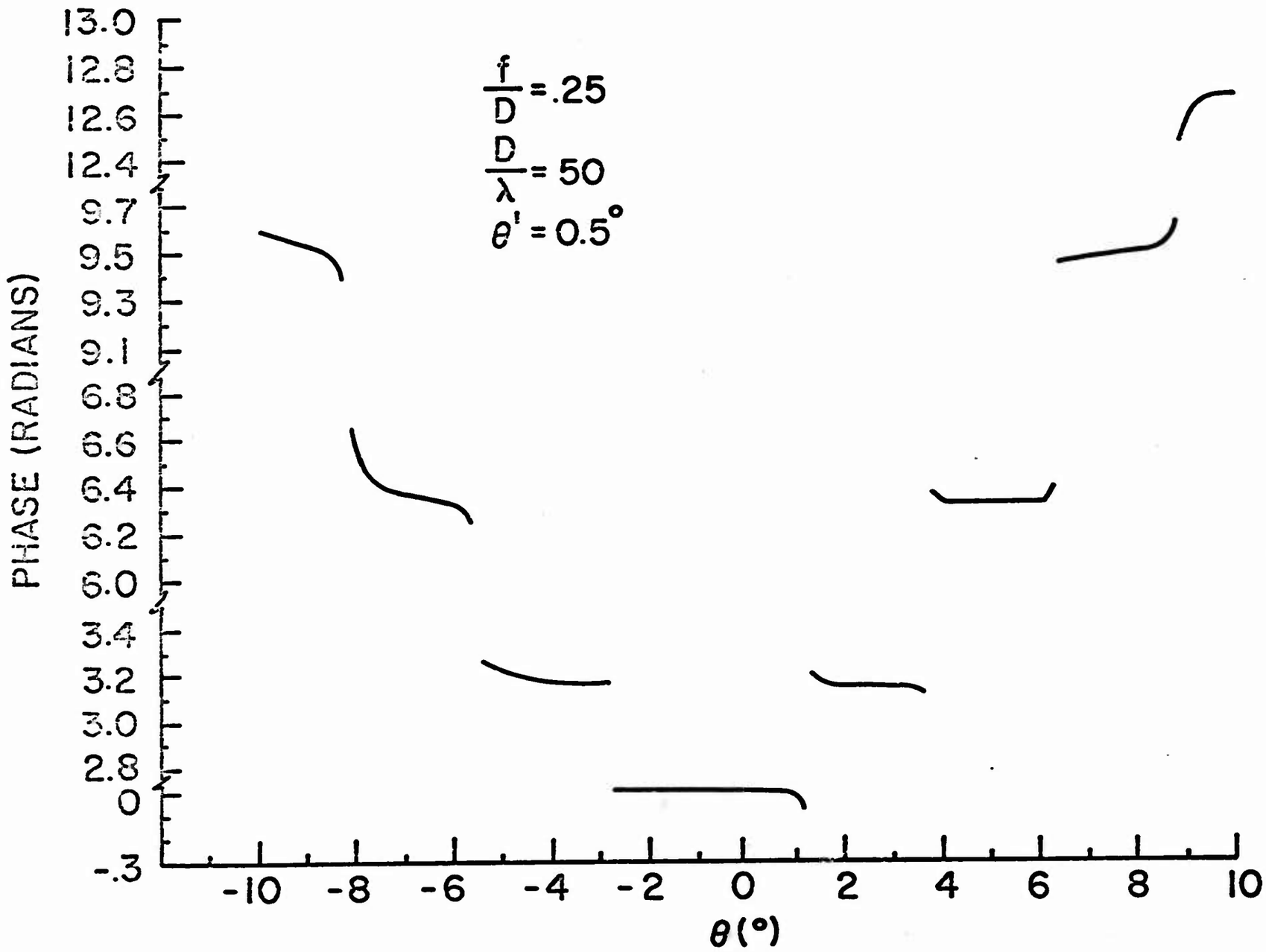

FIG. 15 THEORETICAL PHASE FOR AN ANGLE OF ARRIVAL (0.5°)

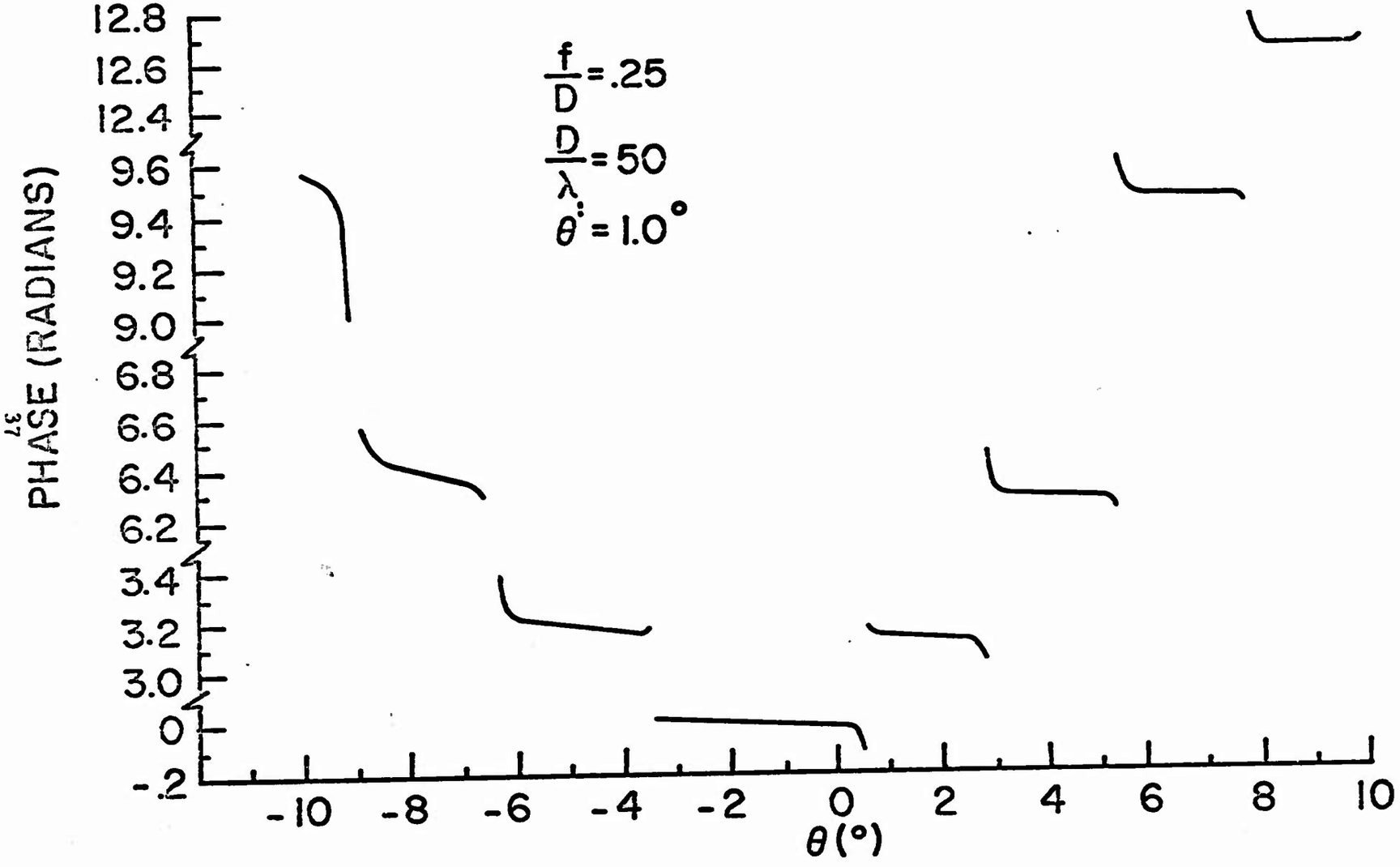

FIG. 16-THEORETICAL PHASE FOR AN ANGLE OF ARRIVAL (1.0°)

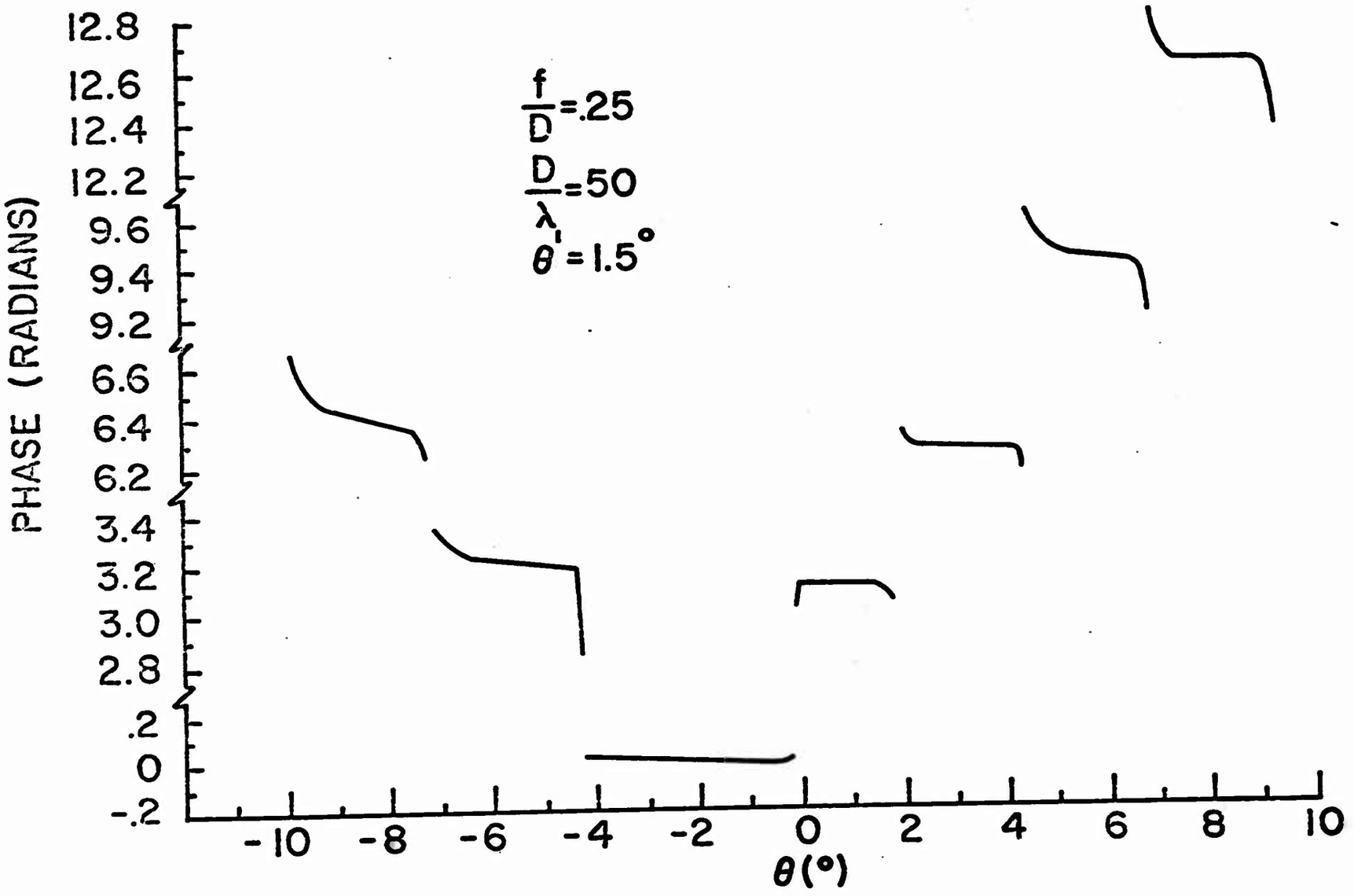

FIG.17-THEORETICAL PHASE FOR ANGLE OF ARRIVAL (1.5°)

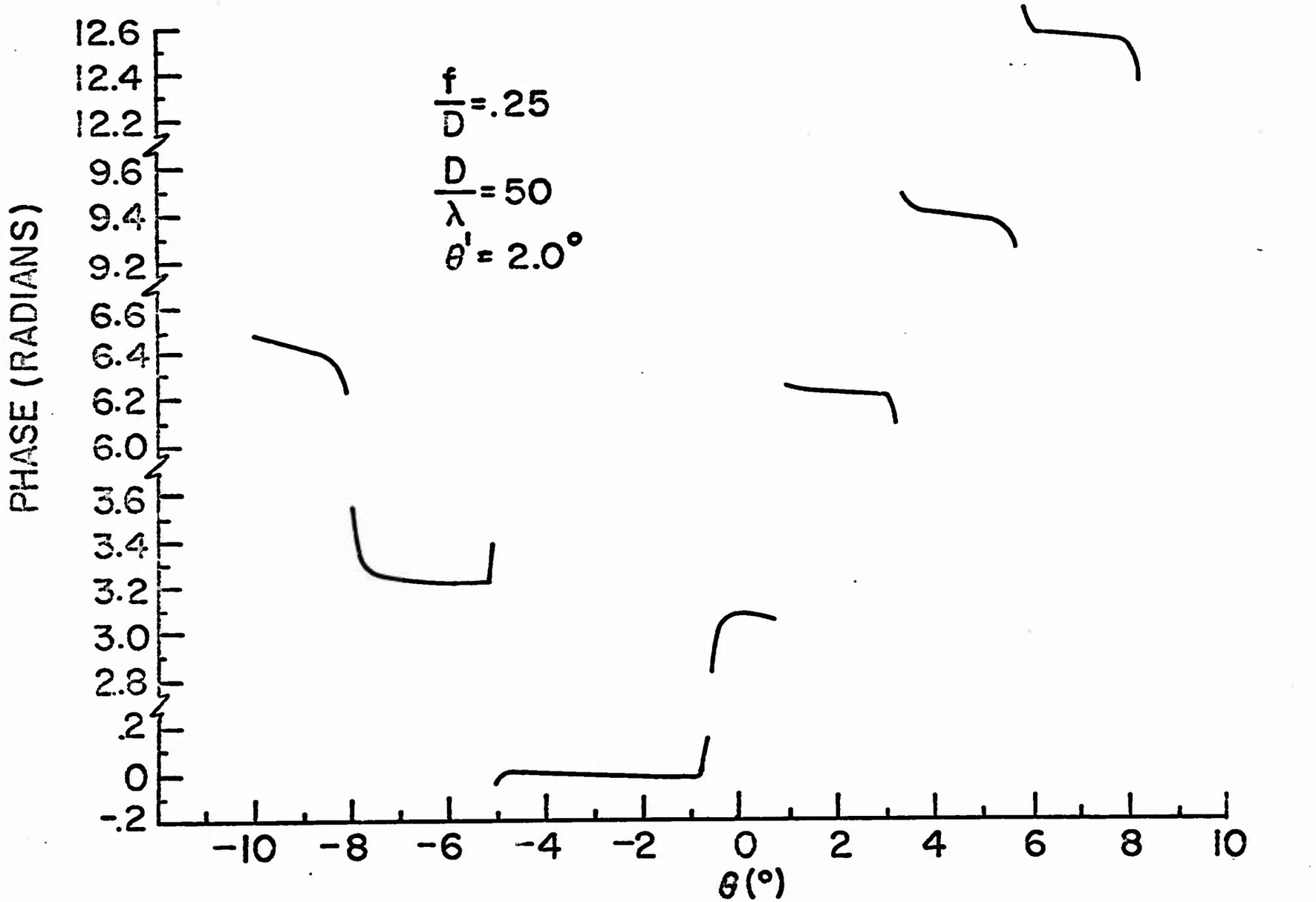

FIG. 18 - THEORETICAL PHASE FOR AN ANGLE OF ARRIVAL (2.0°)

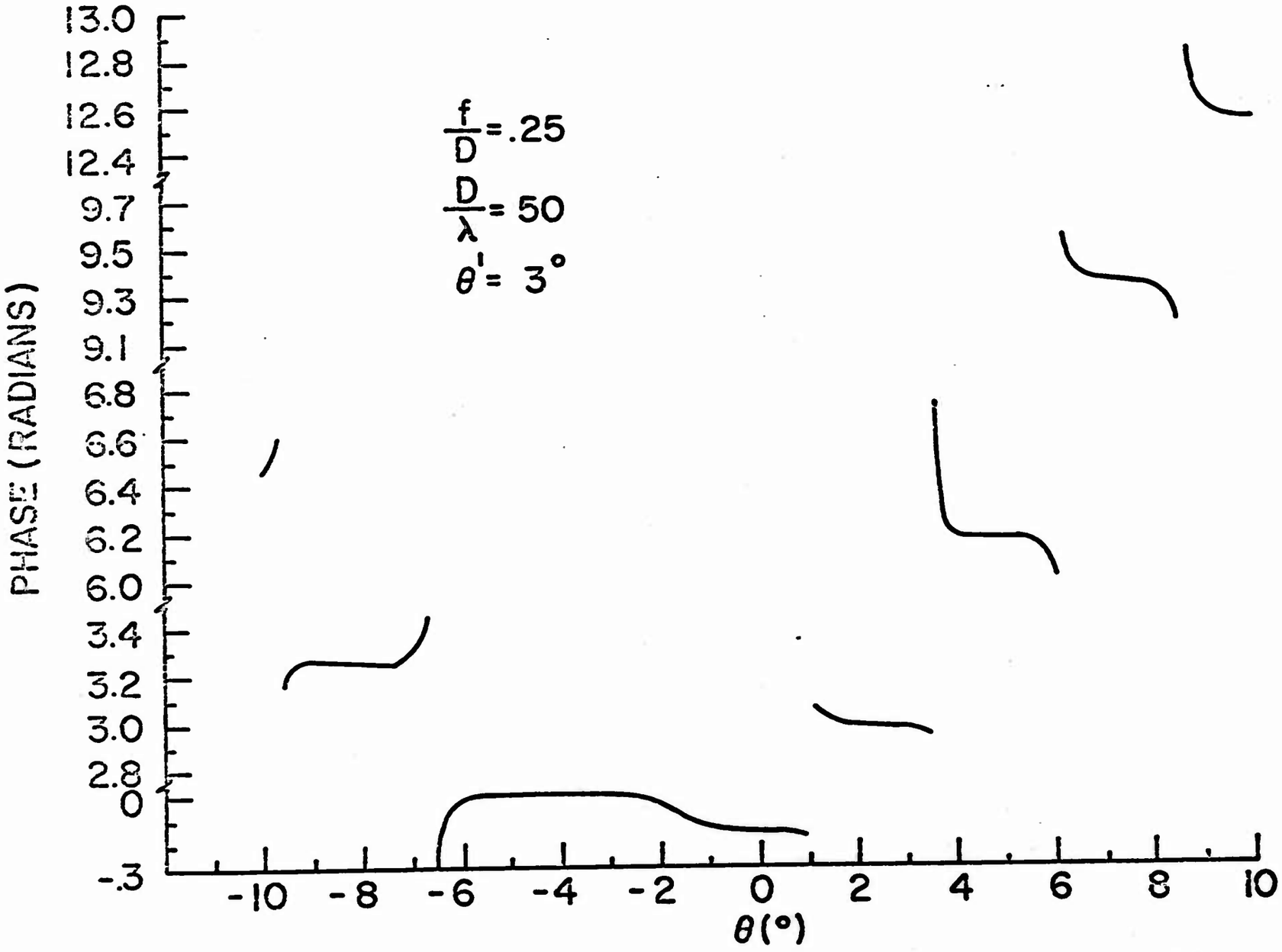

FIG.19-THEORETICAL PHASE FOR AN ANGLE OF ARRIVAL (3.0°)

the angle of arrival. This displacement of the maximum focal plane field intensity is 1.6 times the angle of arrival. The phase distributions still contain the discontinuous steps of about π radians, with a superimposed tilt due to the tilt of the incident wave. Further comments on these diffraction patterns will be made in the Experimental and Conclusions sections of this report.

3. EXPERIMENT

An experiment was designed to measure the focal region fields of an aperture focused in its near field. A structure equivalent to the focused infinite slit is the parallel plate guide containing a lens. This structure propagates a TEM wave, polarized perpendicular to the parallel plates, and only permits diffraction in one dimension. These polarization and diffraction properties agree with the analysis of Section 2.

An artist's conception of the structure is given in Figure 20. In order to keep the physical size within reasonable limits, the experiment was performed at 35 GHz. The lens is plano-hyperbolic and is constructed of Rexolite 1422, having an index of refraction of n = 1.59 at 35 GHz. The spacing of the parallel plates is .088", which insures that only the desired polarization can be supported even in the region of the lens. The total height of the lens is 16.87" (50λ) and the height of the parallel plate structure is 18.87". The two inch differential in height is evenly distributed on either side of the lens, and is filled with absorber in order to approximate the effect of the parallel plates going off to infinity. The probe consists of reduced height RG-96 waveguide to fit between the parallel plates. The aperture size of the probe is .030" x .080". The probe is equipped with a drive mechanism capable of accurate movement in the focal plane.

The circuit used to measure the diffraction pattern is shown in Figure 21. The source is a 1000 Hz square wave modulated, klystron oscillator. The phase and amplitude of the diffracted wave are measured by a bridge circuit. A superheterodyne receiver is needed in order to operate with a reasonably small probe aperture. The 225' spacing between the source and the lens structure more

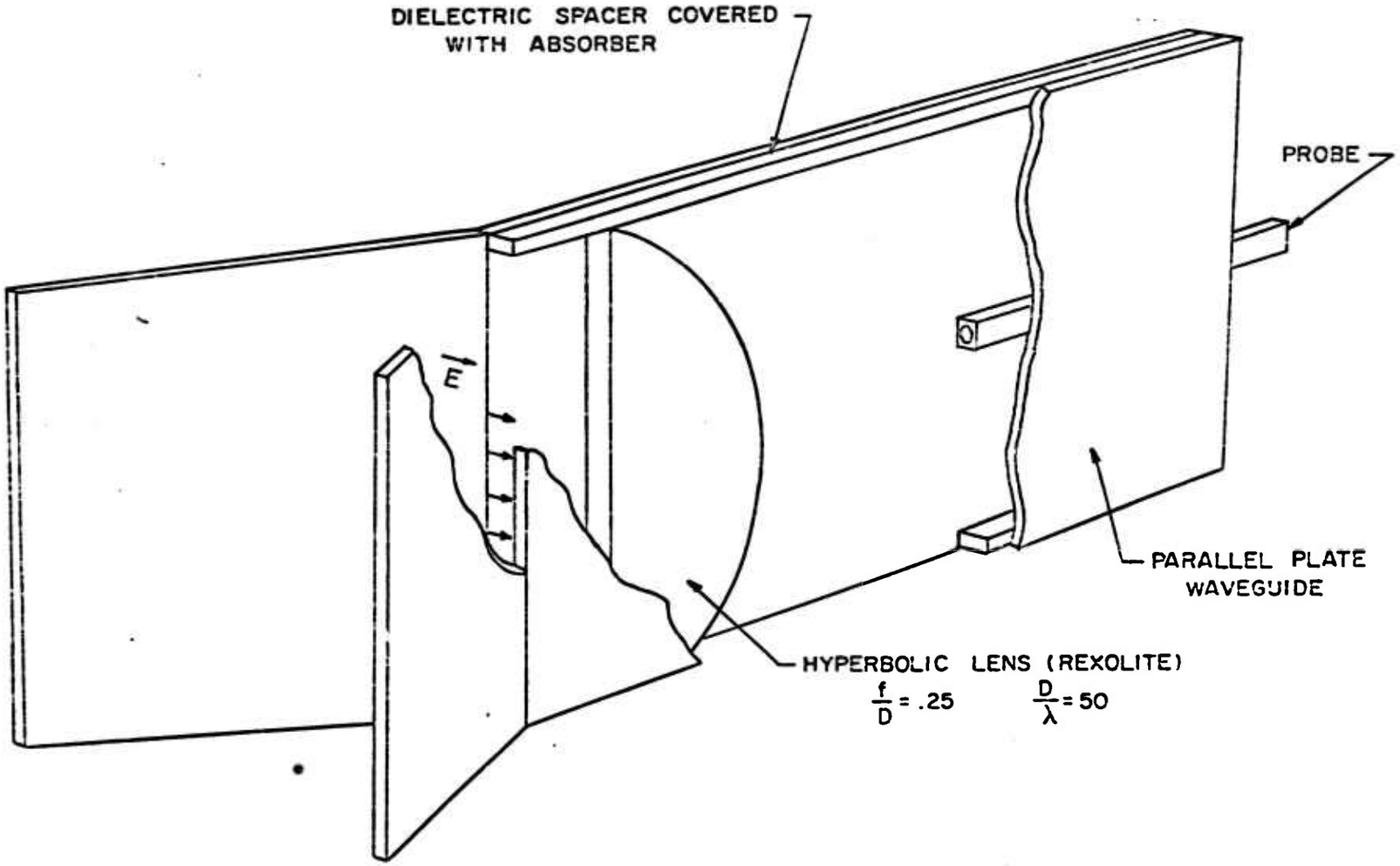

FIG.20 – PARALLEL PLATE – LENS ANTENNA

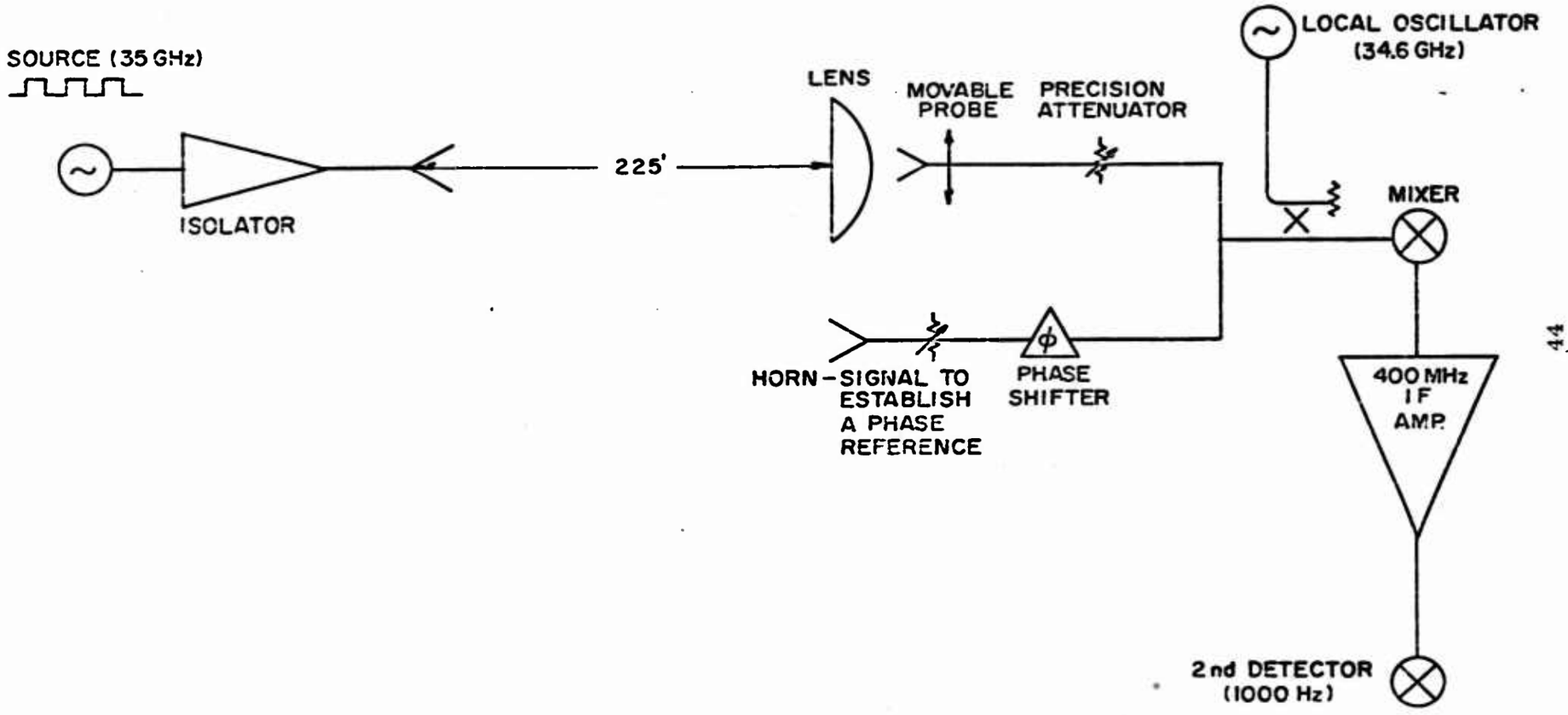

FIG. 21 - SYSTEM FOR MEASURING AMPLITUDE AND PHASE OF THE DIFFRACTION PATTERN

than satisfies the two Rayleigh distances ($\frac{2D^2}{\lambda}$) required for plane wave illumination. Figure 22 is a view of the pattern range, looking from the transmitter toward the test station. The actual arrangement of the structure during measurements is shown in Figure 23. In Figure 24 the parallel plates have been separated in order to show the lens and probe.

Initial measurements were poor due to several effects. Tests on the parallel plate structure without the lens indicated the presence of a large standing wave due to reflections from the rear opening. This was corrected by the addition of an absorber within the backside of the structure, everywhere except where probe motion was required. Reflections at the air-lens interface resulted in a standing wave within the lens. This produced undesired phase variations in the diffracted wave. A non-reflecting coating was applied to the planar surface of the lens. This allowed internally reflected energy to pass out of the structure. There was also a problem with the lens properly contacting the parallel conducting plates. This was overcome by chemically depositing a thin film of silver on the broad-flat surfaces of the lens.

Patterns were measured for normal incidence and for all the angles of arrival for which computations were performed. The results are given in Figures 25 through 30. (In some cases, only the maximum of a sidelobe could be measured, and this is shown as a dot.) A point by point comparison with the calculated data indicates rather poor agreement, although always better than that obtained by comparison with calculations based on the Fraunhofer approximation. However, the qualitative agreement is very good. This is particularly evident for the highly unsymmetric pattern for the angle of arrival $\theta' = 3.0^{\circ}$. Two other interesting comparisons

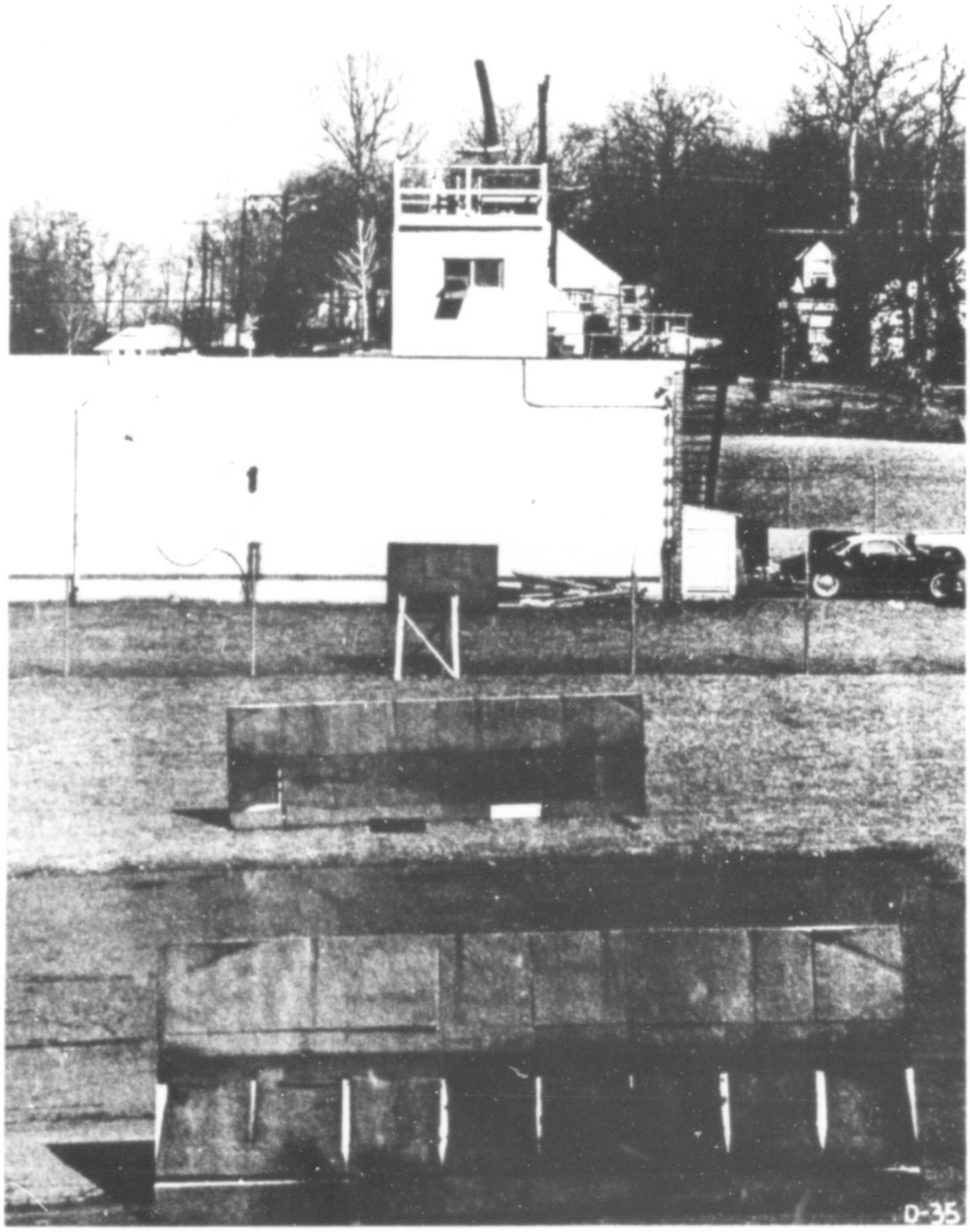

FIG. 22 - A VIEW OF THE PATTERN RANGE
LOOKING FROM THE TRANSMITTER SITE

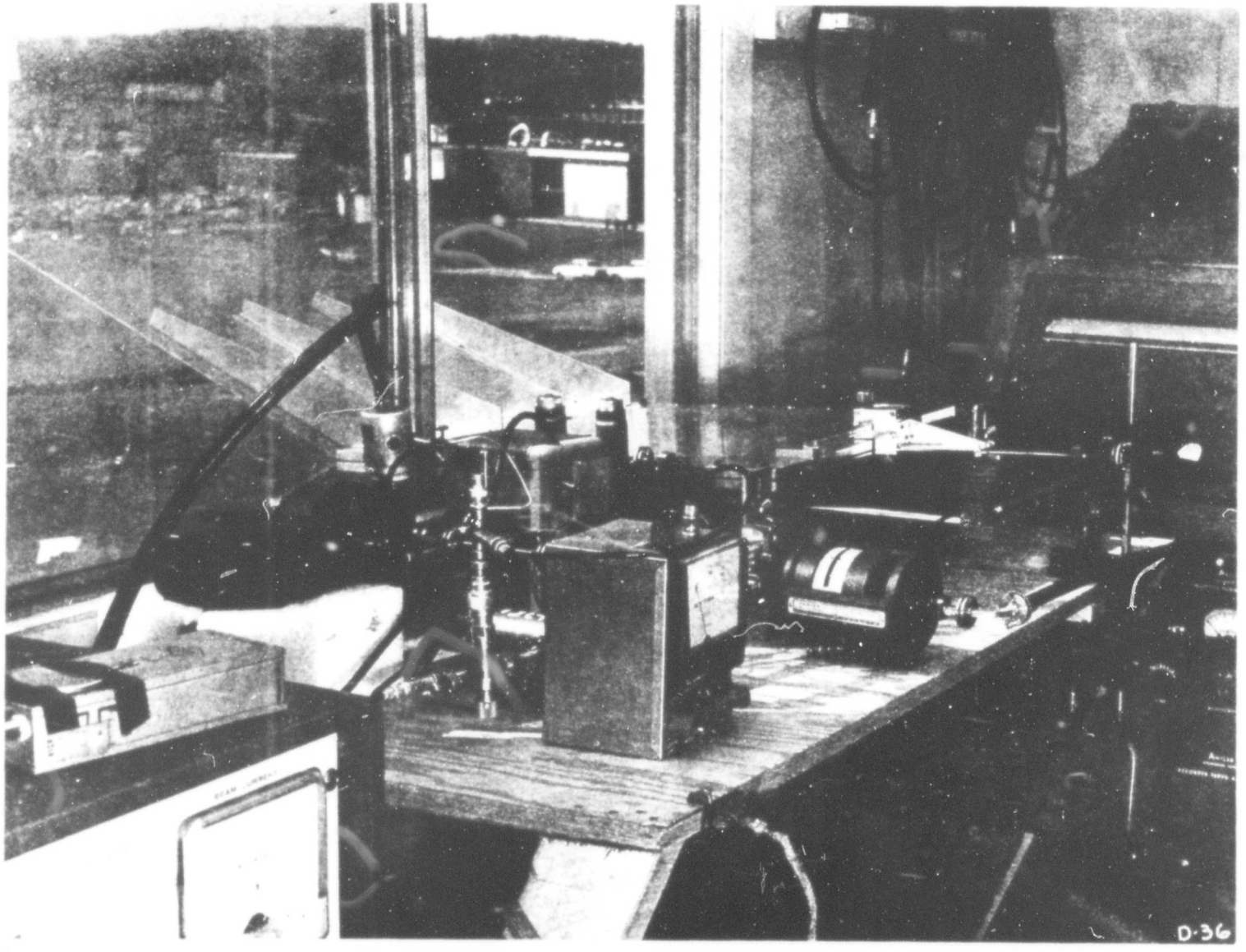

FIG. 23 - A VIEW OF THE MEASURING APPARATUS

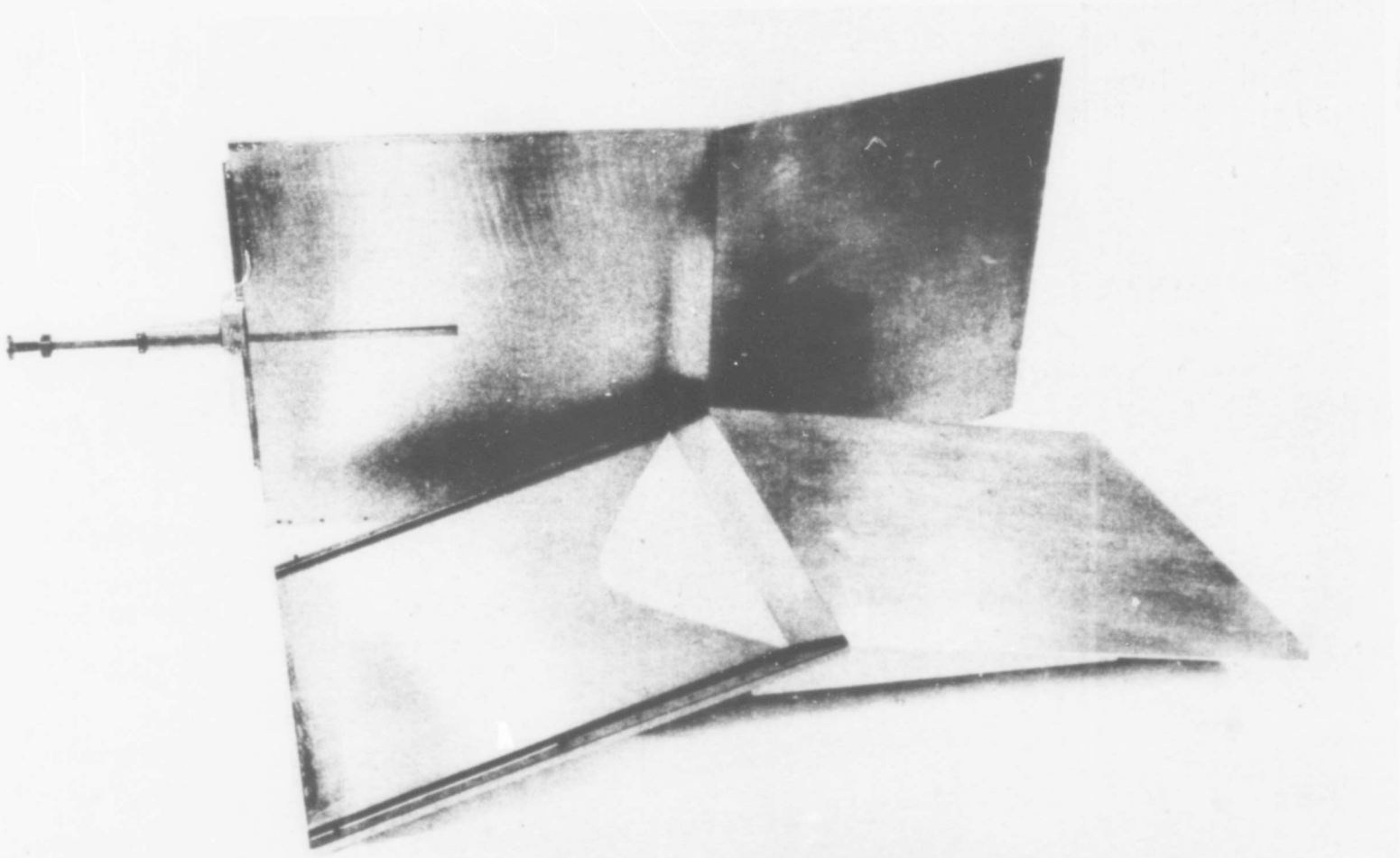

FIG. 24 - THE TEST STRUCTURE WITH THE PLATES SEPARATED TO SHOW THE LENS AND PROBE

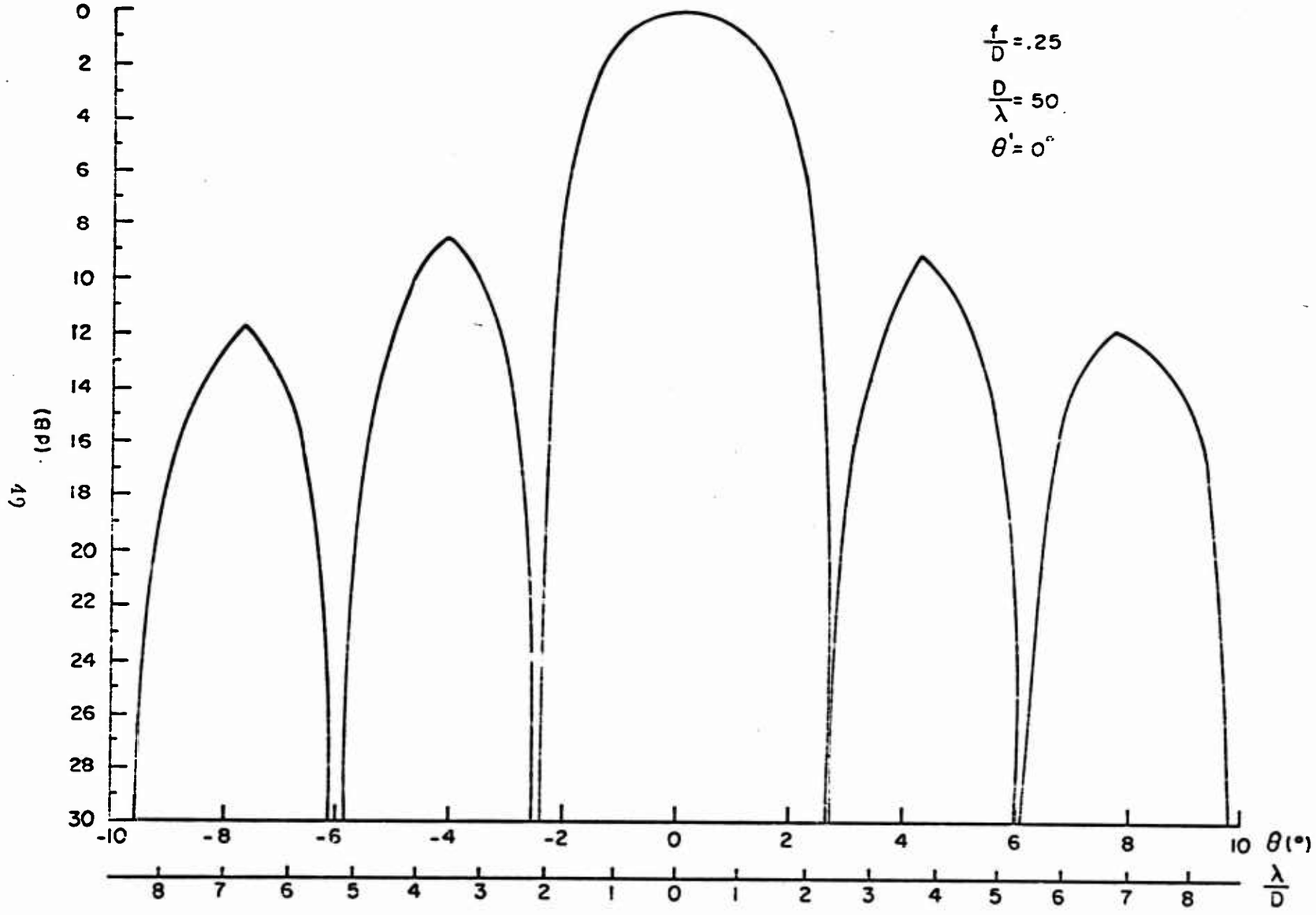

FIG.25- MEASURED POWER PATTERN FOR NORMAL INCIDENCE

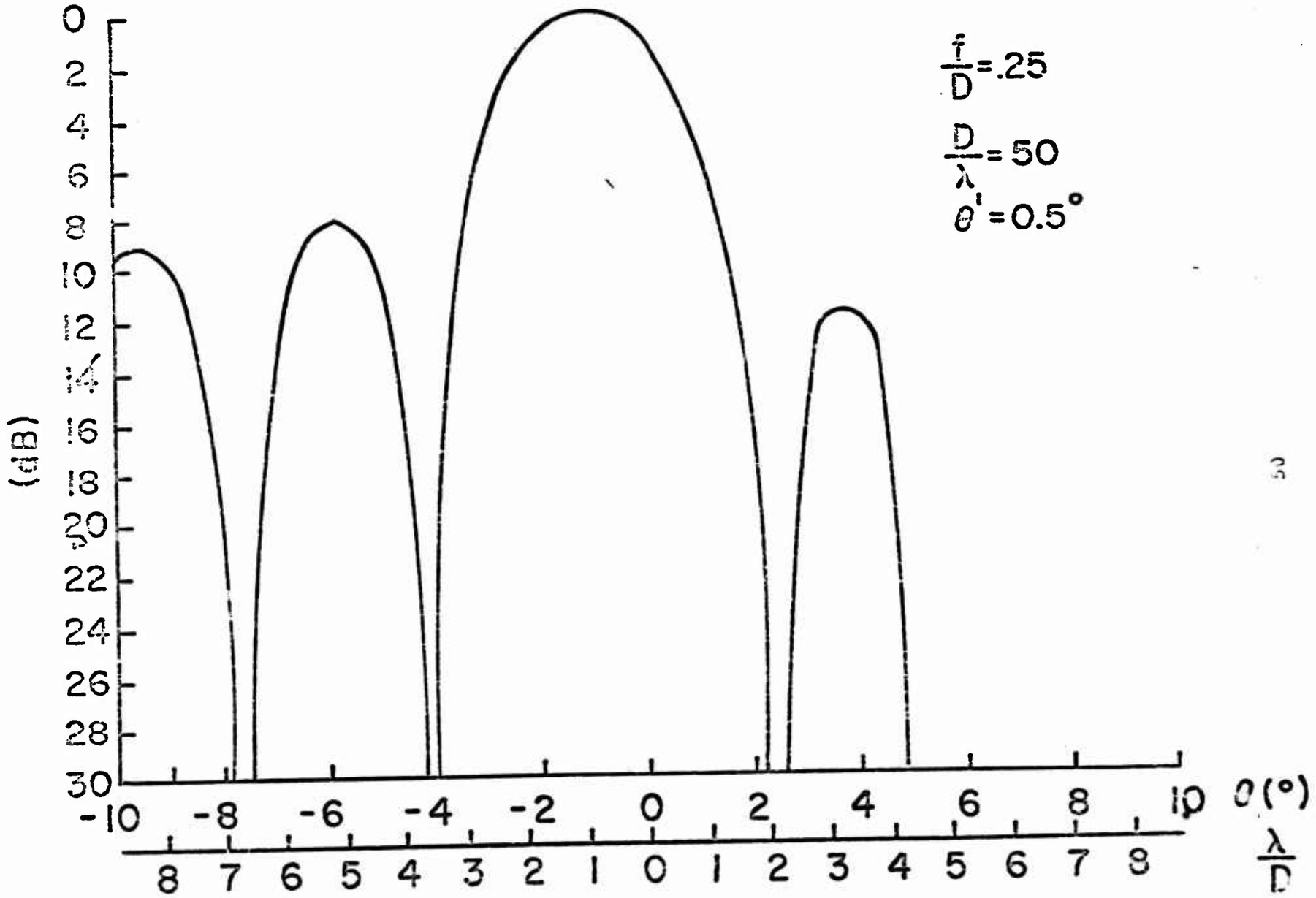

FIG.26-MEASURED POWER PATTERN FOR AN ANGLE OF ARRIVAL (0.5°)

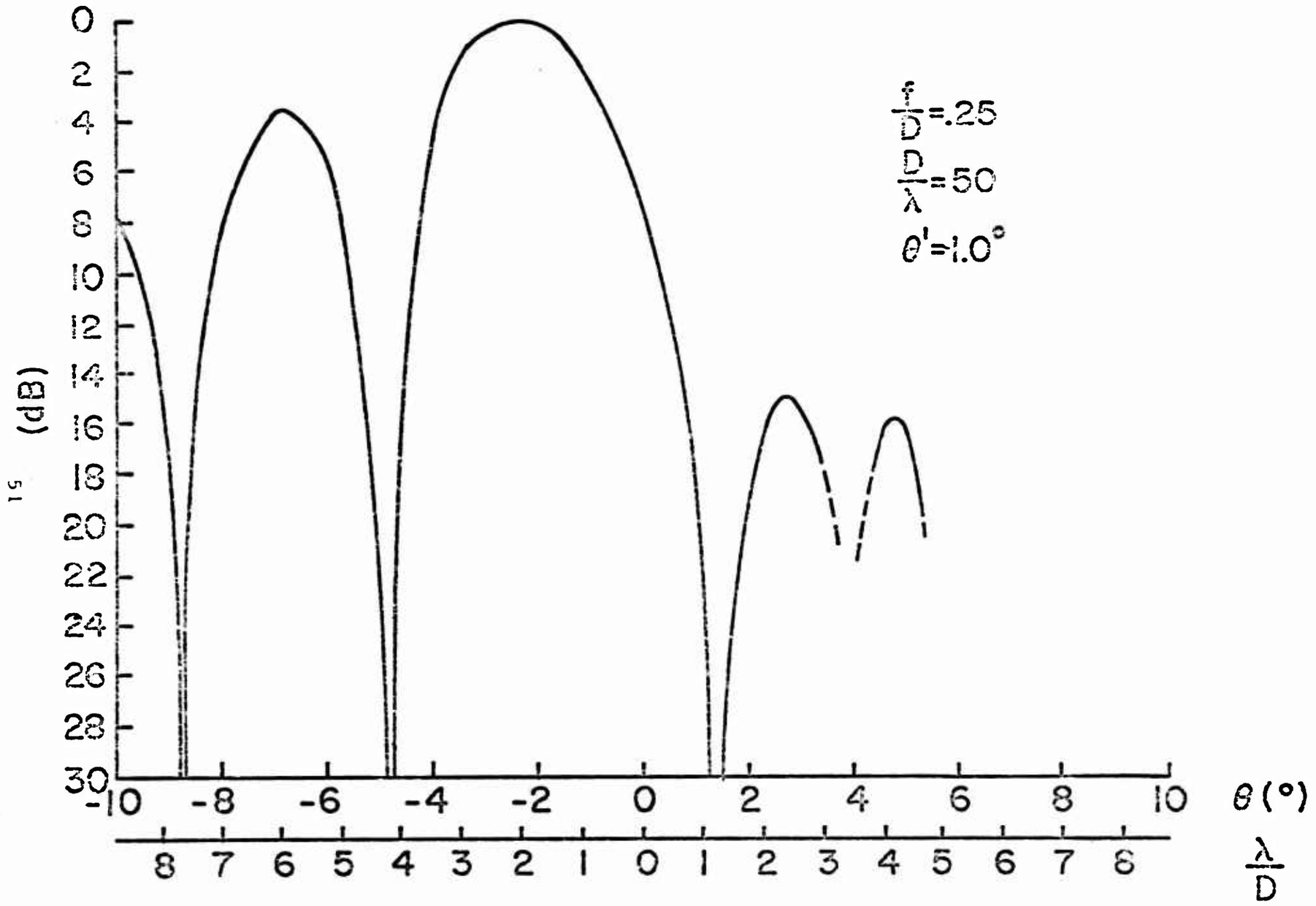

FIG.27-MEASURED POWER PATTERN FOR AN ANGLE OF ARRIVAL (1.0°)

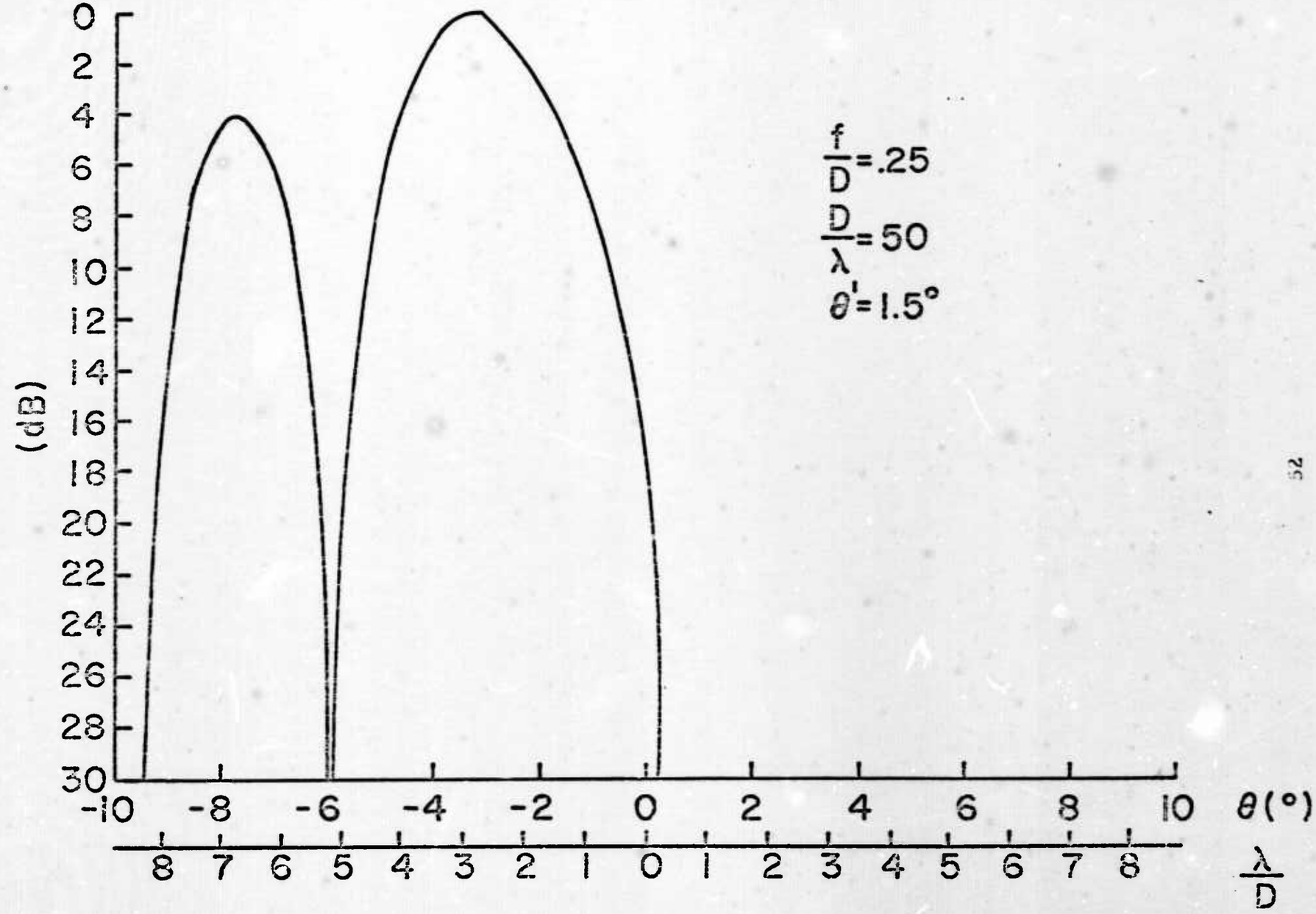

FIG.28-MEASURED POWER PATTERN FOR AN ANGLE OF ARRIVAL (1.5°)

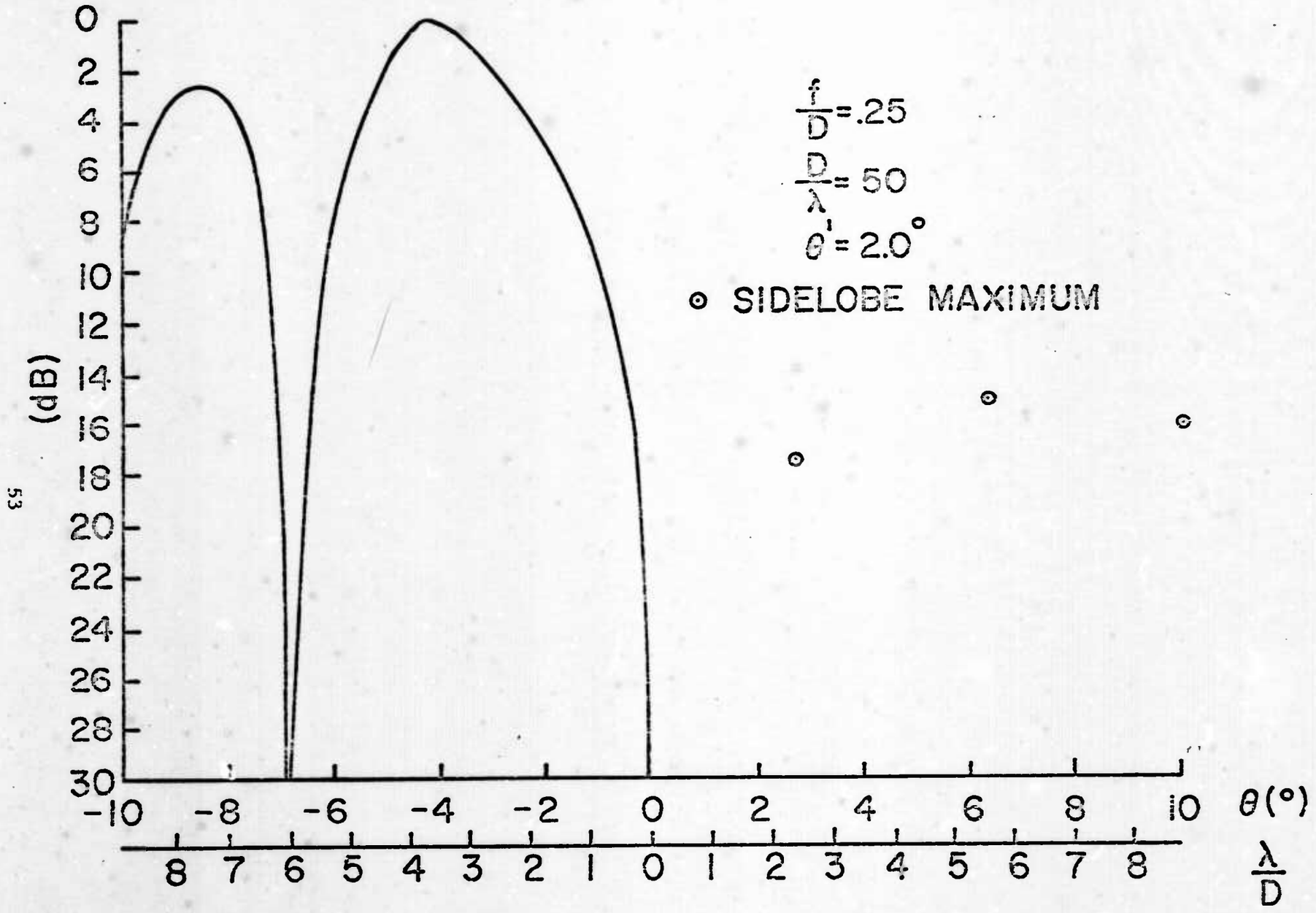

FIG.29-MEASURED POWER PATTERN FOR AN ANGLE OF ARRIVAL (2.0°)

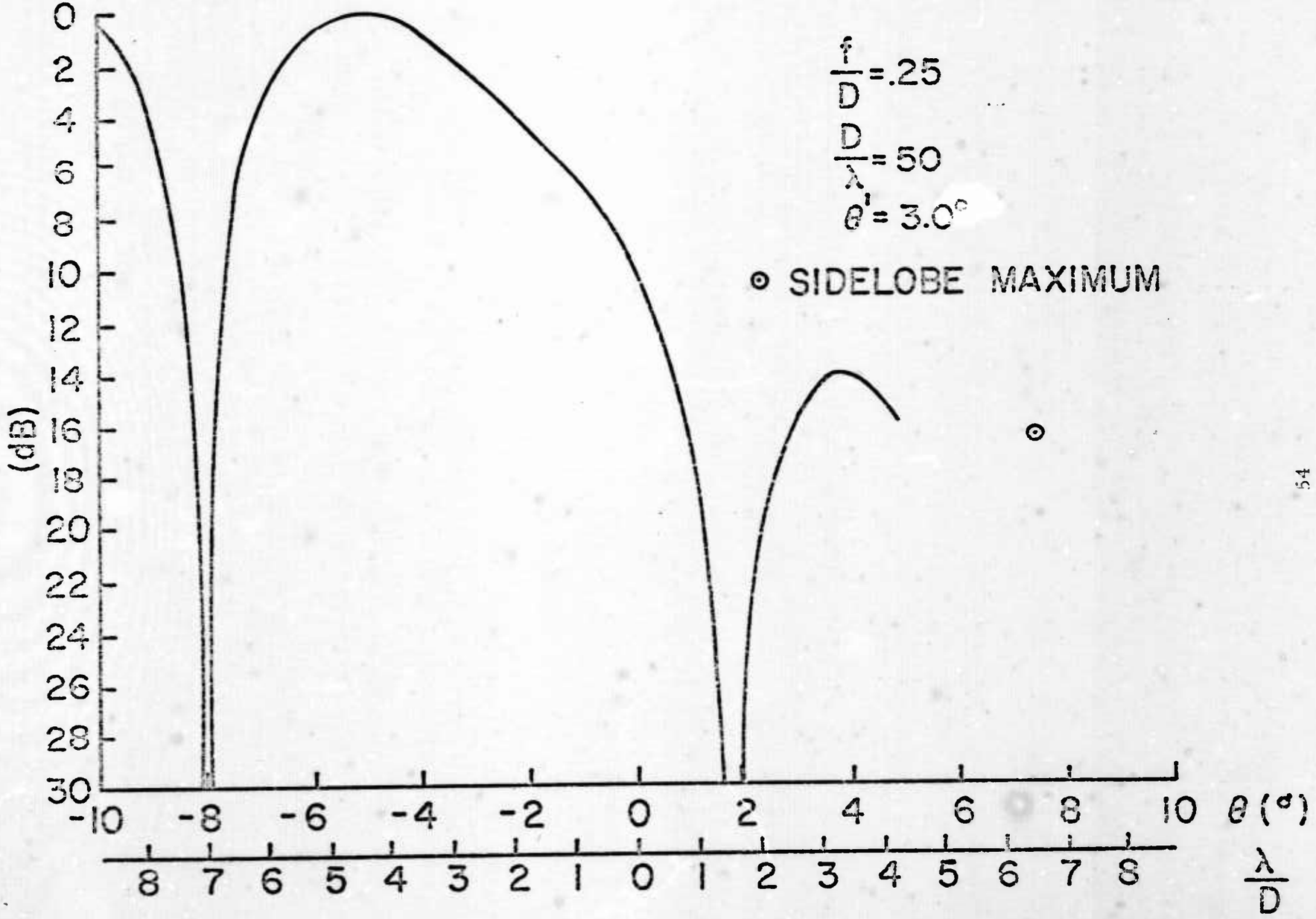

54

FIG.30-MEASURED POWER PATTERN FOR AN ANGLE OF ARRIVAL (3.0°)

can be made between the calculated and measured patterns. The calculated patterns were presented in a normalized form. The computer solution was in a non-normalized form permitting direct comparison of power for different angles of arrival. A curve of the power at the maximum of the diffraction pattern (relative to that at $\theta = 0$ when $\theta' = 0$) versus the angle of arrival is given in Figure 31. The measured data is in very good agreement in both magnitude and shape. The other comparison is the displacement of the angle of the diffraction maximum (θ MAX) versus the angle of arrival. The Fraunhofer approximation would predict a one-to-one relationship. Our analysis predicts that for angles of arrival up to about 2.0°, the ratio of displacement is 1.6. The measured data yields a ratio of 2.2. These results are shown in Figure 32. Measured phase data has not been included in these figures because the system signal-to-noise ratio did not permit accurate phase measurement. However, the abrupt steps of about π radians were observed to correspond to the position of power nulls.

There is more than a casual agreement between this measured data and the calculations. There are two fundamental departures from the calculations; (1) the measured patterns are spread in comparison to the calculations, and (2) the angular displacement of the diffraction maxima are too large. This has prompted an in depth study of the experiment for sources of error, their potential magnitude, and the direction of the resulting effects.

As with any experiment involving field probing, the probe must be considered as a source of experimental error. Because of our limited receiver sensitivity, we were forced to operate with a probe aperture which subtended an angle of 1.1° in the focal plane. The integrating effect of the probe makes the accurate measurement of the position of nulls and the particular shape of the pattern

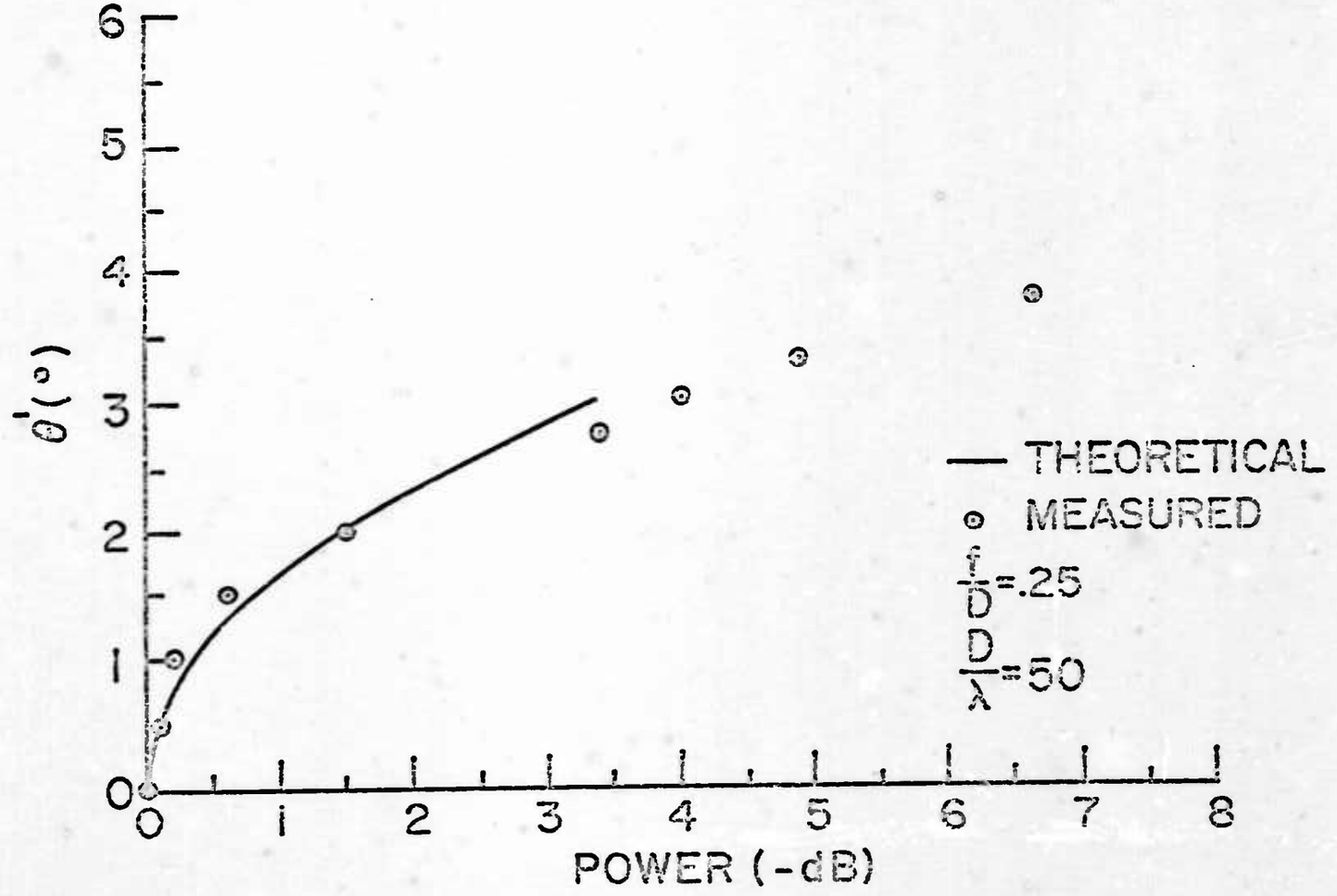

FIG.31 - POWER AT THE MAXIMUM OF THE MAIN BEAM VS ANGLE OF ARRIVAL

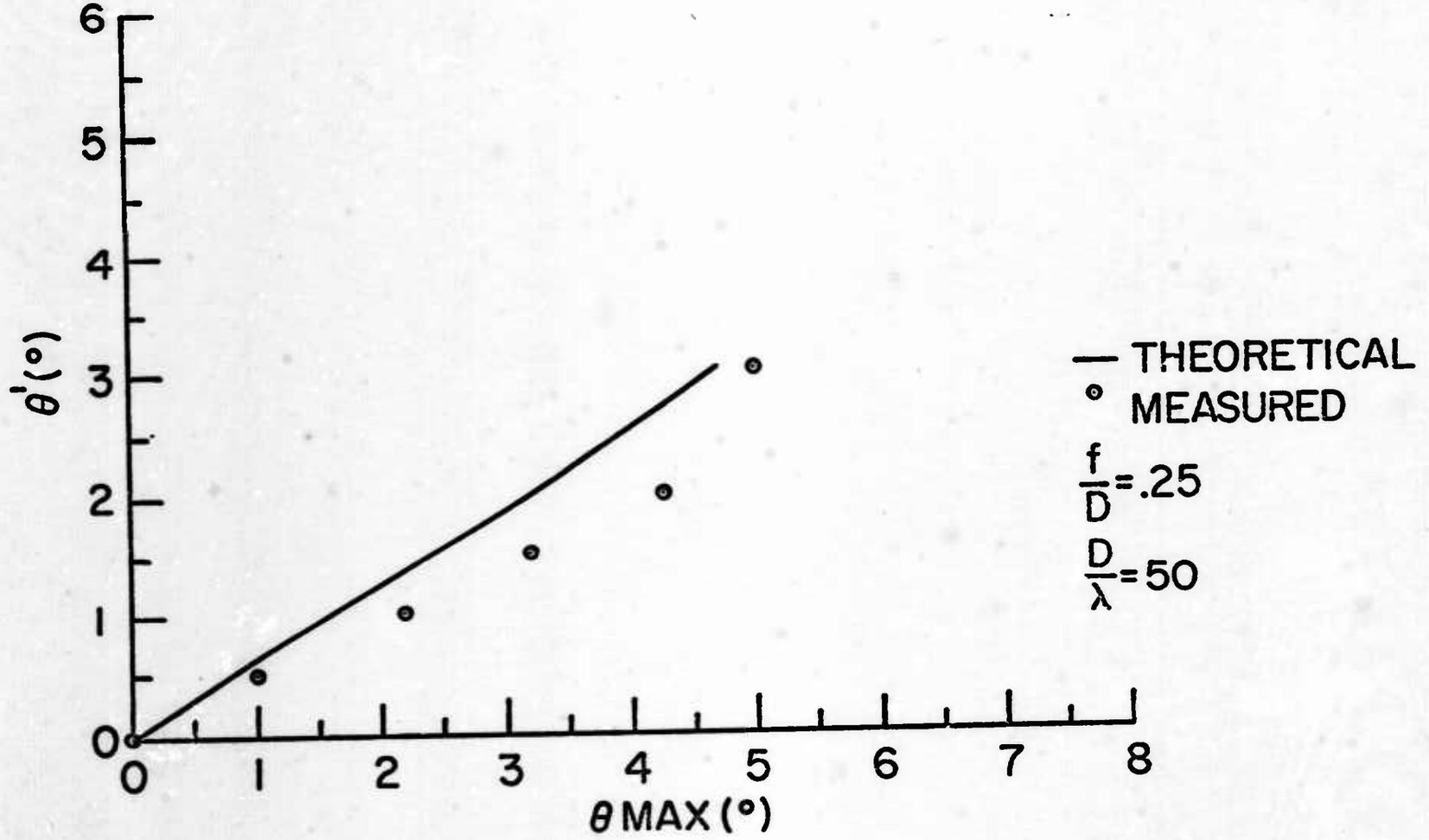

FIG.32-ANGULAR DISPLACEMENT OF THE MAIN BEAM VS ANGLE OF ARRIVAL

(3 dB points, etc.) very difficult. Also, the manual movement of the probe necessitated a quantized measurement of the pattern. The data was presented exactly as measured, and hence, some of the sidelobes appear pointed.

An even more fundamental problem exists in the design of the lens. In an effort to avoid amplitude tapering due to loss in the lens material (the analysis assumed uniform amplitude illumination), a low dielectric constant material was used. This resulted in a thick lens, for which the principal plane (effective aperture plane) location is not accurately known. The indications are, from applying techniques of ray optics, that the effective aperture of our lens is less than the desired 50λ.

A further complication arises from the radiation pattern of the probe itself. An isolated measurement of the probe revealed that it introduces a 3 dB taper out to the 45^{o} point of its radiation pattern. This superimposes an amplitude taper across the aperture and would have the effect of spreading the pattern.

Because of the mutual interplay between the probe and the lens, it was felt that the question of determining the effective aperture could best be answered by direct measurement of the entire structure's far field pattern. With the probe fixed on the axis of the lens, rotation of the entire structure should produce the Fraunhofer far field pattern. The results are given in Figure 33. The first null occurring at about 2^{o} indicates that the effective aperture is about 30λ. The location of the focal plane of the structure was verified by measuring a series of diffraction patterns through several planes, and determining the plane for which the width of the main beam was a minimum. This corresponded exactly to the predicted location of the focal plane. The combined

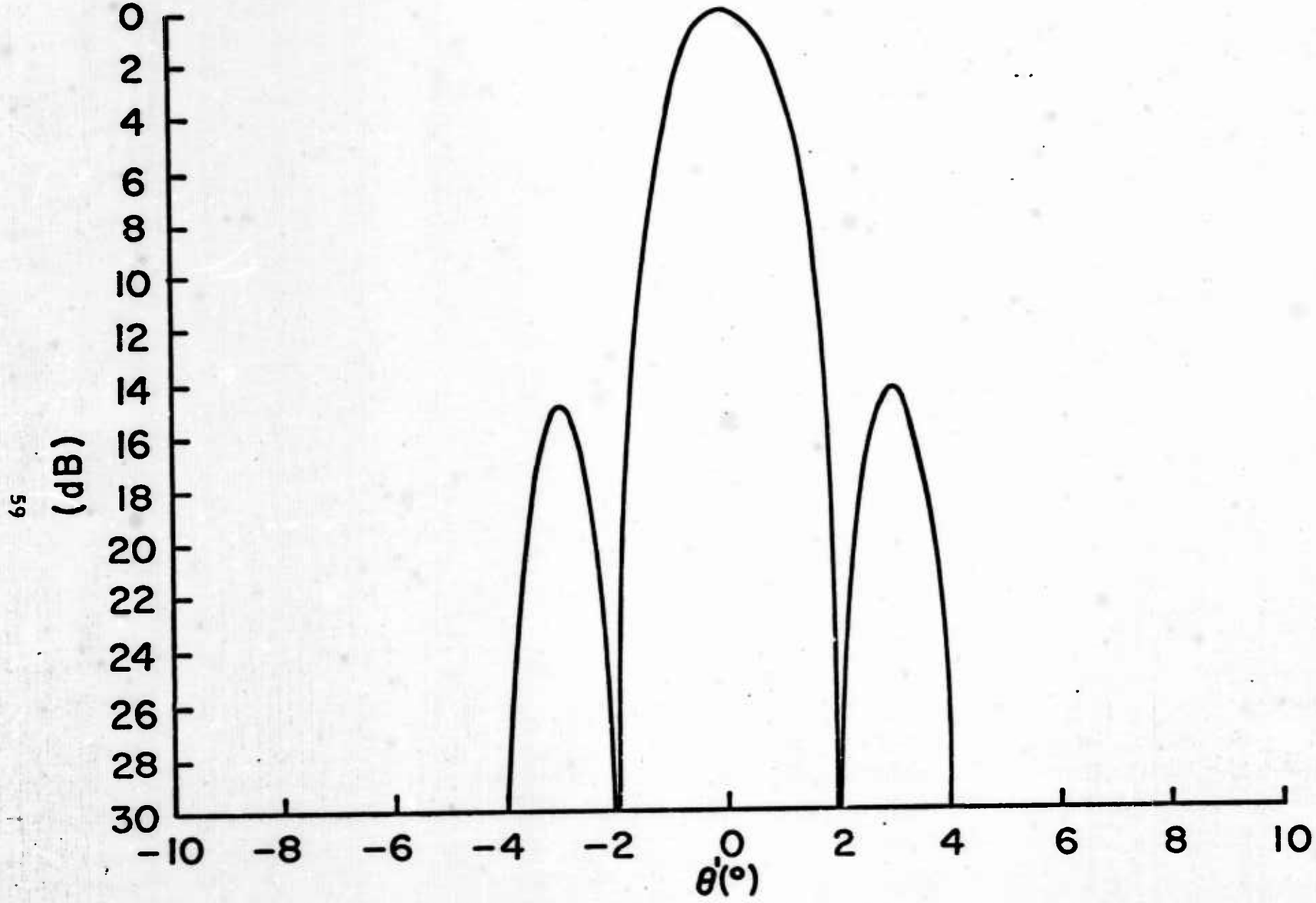

FIG. 33-THE FAR FIELD PATTERN OF THE PARALLEL PLATE-LENS STRUCTURE

result is that the experimental structure has an f/D too large and a D/λ too small. The f/D is approximately .57 which is still in the near field and hence in the region of interest. The D/λ is approximately 30. Lacking a solution of Equation (64) for this value, we can only say that it is in the correct direction to account for the variations in the measured and calculated patterns.

This problem was alluded to in Section 2 when it was noted that caution is required in going from the mathematical model of a focused aperture to some real structure. The model assumed that all phasing was accomplished in an infinetesimal region called the aperture plane. This is not the case in lenses or reflecting antennas. The application of Equation (64) to some particular structure will first involve determining the correct f and D. Another result of the focusing model is its inability to correctly account for the skewed path through a lens or parabola due to off axis illumination. To include this effect would amount to an unnecessary complication for the small angles of arrival which are of interest.

4. CONCLUSIONS

Let us assume in this discussion that all the apertures of interest are very large ($D >> \lambda$) and that the diffraction angles of interest are small. As previously stated, this allows one to neglect polarization (essentially treating the principal polarization) and confine all further discussion to the scalar approximation. Under this assumption, the exact solution for the focal region fields, resulting from complex amplitude and phase distributions in the aperture plane, requires solving an integral of the product of the aperture plane distribution and the aperture transformation function. This requires a computer solution for each aperture plane distribution. We feel that a more manageable approach is the statistical combination of an ensemble of plane waves. The weighting factor (the relative amplitude and phase between component waves) is determined by the nature of the aperture distribution. In principal, the component plane waves could have any angle of arrival from the forward hemisphere. This will also be a function of the type of aperture error. The simplification of this approach arises from the fact that once the integral of the aperture transform function is solved for a given angle of arrival, different aperture plane distributions can be solved by an algebraic manipulation of the component waves, weighted with appropriate phase and amplitude.

Prior to treating particular aperture plane distributions, it was necessary to develop the aperture transform function for apertures focused in their near field. Very significant results came from this investigation. The diffraction characteristics of a single plane wave were substantially different from the Fraunhofer approximation. The main beam is much wider and the sidelobe level is higher than customarily assumed. For very small angles of arrival,

the shape of the main beam remains constant, but it is displaced by an angle greater than the angle of arrival. This is significant to the design of an adaptive feed system since, even through the aperture plane errors only excite small angular waves, these angles are exaggerated by diffraction. This could result in the angle subtended by the feed structure being considerably larger than the cone of angles of the plane waves required to synthesize the aperture distribution. The final design of the feed system will be predicated on the granularity of the interference pattern of this ensemble of plane waves. This will determine the number of elements required to recover a given percentage of the energy in the focal plane. The size and location of the elements in the focal plane must be chosen so as to produce the minimum disturbance of the focal region fields.

The final determination of the focal region field structure for a particular aperture distribution will require the complex addition of the constituent plane waves. There has not been sufficient time to investigate these ensemble characteristics during this contract. However, one particular aperture distribution of interest has been set up to demonstrate the technique. A periodic aperture distribution, with a period greater than the wavelength of the incident radiation, can be represented by the superposition of two plane waves. The magnitude of the aperture plane variations will be determined by the relative amplitude of the two incident plane waves. The period of the aperture plane variations will be determined by the angles of arrival. Assume a reference wave, which after diffraction has the form

$$U_{P_o}(\theta_1') = A_o(\theta_1') + i\, B_o(\theta_1') \quad . \qquad (75)$$

The second wave, which produces the desired interference pattern, has the form,

$$U_{P_1}(\theta_2') = \left[A_1(\theta_2') + i\,B_1(\theta_2')\right] e^{\,i\Delta\phi} \quad , \tag{76}$$

where $\Delta\phi$ is the initial phase difference between the two waves. This determines where in the aperture plane the maxima of the periodic variations occur. The magnitude of the variations will depend on the amplitude ratio a_1, where,

$$E_1(\theta_2') = a_1 E_o(\theta_2') \quad ; \tag{77}$$

resulting in,

$$A_1(\theta_2') \rightarrow a_1 A_o(\theta_2') \quad , \quad B_1(\theta_2') \rightarrow a_1 B_o(\theta_2') \quad . \tag{78}$$

The A's and B's are the real and imaginary solutions of Equation (64) for the particular values of θ'. The total resulting field in the focal plane is given by,

$$U_P = A + i\,B \quad , \tag{79}$$

with

$$A = A_o(\theta_1') + a_1\left[A_o(\theta_2')\cos\Delta\phi - B_o(\theta_2')\sin\Delta\phi\right] \quad , \tag{80}$$

$$B = B_o(\theta_1') + a_1\left[A_o(\theta_2')\sin\Delta\phi + B_o(\theta_2')\cos\Delta\phi\right] \quad . \tag{81}$$

The diffraction pattern can be found from Equations (80) and (81), and is given by,

$$|U_P|^2 = |U_{P_o}(\theta_1')|^2 + a_1^2\,|U_{P_o}(\theta_2')|^2 + 2a_1\left\{A_o(\theta_1')\left[A_o(\theta_2')\cos\Delta\phi - B_o(\theta_2')\sin\Delta\phi\right] + B_o(\theta_1')\left[A_o(\theta_2')\sin\Delta\phi + B_o(\theta_2')\cos\Delta\phi\right]\right\} . \tag{82}$$

The zero subscripts refer to the calculations performed in Section 2 assuming unit incident amplitude, $E_o = 1$. The first two terms on the right hand side of Equation (82) are ordinary diffraction patterns for particular angles of arrival (θ'), like those presented in Figures 10 through 14. The last term in Equation (82) would require some algebraic calculations. The necessary A's and B's have been included as print outs in the computer program.

Even this simple example demonstrates that for combining more than two waves, the algebra can become quite tedious. However, in principal it can be solved on a desk calculator, whereas the exact problem cannot. In some cases, when many waves are to be investigated, it would be simpler to include the performance of Equation (82) in the computer program.

Aside from developing the tool for treating the problem of distorted apertures, the analysis in this report provides an excellent approximation for the behavior of assumed perfect apertures focused in their near field. The analysis was tested by performing experiments, and, although the experimental structure did not exactly correspond to the parameters used in the analysis, the qualitative agreement was good. The analysis predicted that for an $f/D = .25$ and $D/\lambda = 50$, the main beam would be 1.74 times larger than the Fraunhofer approximation. Other experimenters have noted and reported this effect. Loux et. al.[9] measured patterns in the near field of a parabolic dish with $f/D \approx .33$ and $D/\lambda = 50$. They found that the radius of the Airy disc was 1.5 times the predicted (Fraunhofer) value. As f/D increases, our

---

9. Loux, P.C., et.al., "Transverse Antenna Feed Study," Sperry Gyroscope Company Final Report on AFCRL Contract No. AF 19(628)-2759; January 1966, p. 20.

analysis yields results which approach those predicted by the Fraunhofer approximation. Hence, the variation in the 1.5 ratio of Loux and our 1.74 is accounted for by the f/D going from .33 to .25. The enlargement of the main beam and the increased sidelobe level are sufficient to justify attempting to recover this energy. Based on the over simplified approach of planimetering the area under a focal plane curve of absolute power, it appears that a feed designed to properly add the main lobe and the first sidelobes would have an efficiency gain of 2 - 2.5 dB over a single feed designed to collect the main lobe predicted by the Fraunhofer approximation. Because the off axis illumination indicated highly unsymmetric sidelobe levels and a steering factor of 1.6, these considerations should yield improvements in the design of monopulse and conical scan systems.

A potentially interesting application of the results of the analysis is its use in the design of feed structures to synthesize prescribed far field radiation patterns. Given a pattern requirement, one can approximate it as an ensemble of incident waves whose individual amplitudes and phases correspond to those of the required pattern at the appropriate angles of arrival. Using the aperture transform developed during this program, the focal plane field distributions of each of these incident waves are calculated and superimposed. A feed assembly is then designed to approximate this focal plane field distribution. This is analogous to the work of Woodward[10] for pattern synthesis by arrays.

---

10. Woodward, P.M., "A Method of Calculating the Field Over A Plane Aperture to Produce a Given Polar Diagram," Journal of the Institute of Electrical Engineers, 93, Part IIIA, 1947, pp. 1554-1558.

5. RECOMMENDATIONS

The aperture transform function developed during this study provides an excellent approximation to the focal region fields of apertures focused in their near field. It provides the basic tool for the study of focal region field dependence on complex aperture plane distributions. Although time did not permit an in depth study of aperture distributions, the effort has progressed to the point where data pertinent to focal plane adaptive combining can now be generated. A program, which makes maximum use of what has been developed, will be given for the continuation of study.

Since the antennas of interest are of the large dish variety, computations should be performed for Equation (33) of the circular aperture. This will determine the nature of sidelobes, steering angle ratio, and phase relationships, similar to the data presented for the focused infinite-slit. This type of data is necessary in order to determine the resulting field granularity from the superposition of the several waves required to synthesize the aperture plane distribution. The design of an array of feed elements is based on the maximum recovery of energy, while introducing a minimum disturbance to the focal region fields. This may not correspond to a plane array located in the focal plane of the dish. The optimum size and location of elements can only be determined when the fields in the focal "region" are known. It is felt that a three dimensional picture of the field structure is needed. This can be accomplished by the simple adjustment of Equation (33) to solve for the field structure in cuts other than the focal plane. This would also answer the question of how critical is the location of individual elements. It is known[2] that the "depth of focus" (distance between the axial 3 dB points) decreases with decreasing

focal length in the Fraunhofer approximation. This situation may be more acute for apertures focused in their near field since both amplitude and phase determine the diffraction pattern. Some further advantage, in terms of aperture blockage, might be realized by locating the elements over a curved surface. Again, Equation (33) is easily set up to solve for this case, provided the curved surface is reasonably regular.

Since it is known that the Fraunhofer approximation for the diffracted fields is good for apertures focused in the Fresnel region, it would be desirable to have a better determination of where the Fresnel-near field boundary occurs. This can be accomplished by solving for other f/D ratios. This would also make the results of this analysis applicable to a wider variety of dishes.

In many cases, the antenna designer is not concerned with aperture plane errors. This would be the case where the reflector surface is reasonably good at the operating frequency and the aperture size is small enough that atmospheric induced errors are not substantial. It might be desired to amplitude taper in order to reduce sidelobe level or alter the main beam characteristics. Our analysis provides a more accurate aperture transform function than the Fourier transformation. The unit amplitude distribution, assumed in our analysis, can be replaced by certain simple distributions (such as the cosine on a pedestal) without appreciably changing the computer effort to solve Equation (33). This would determine the phase and amplitude distribution required in the focal plane to produce the desired aperture plane amplitude distribution.

It will be desired to experimentally verify many of the above calculations. During the experiments already performed, it was

found that the existing thick lens was a poor approximation to the model for which calculations were performed. Since the structure represents a simple technique for testing the limits of applicability of the analysis, it is recommended that the existing lens be replaced by a thin lens, whose effective aperture and focal length are more easily determined. The geometry will remain plano-hyperbolic because of the reduced machining when only one curved surface is involved. The use of a higher permittivity material will reduce the lens thickness to a more reasonable size. As an example, Emerson & Cuming, Inc., Hi K #140 has a dielectric constant of 20 and a loss tangent of .0009. A lens with $f/D = .25$ and $D/\lambda = 50$ would have a maximum thickness of 3.89λ. The amplitude taper introduced by lens loss would be 0.43 dB.

Based on the results of this program, the use of a corrected lens should result in very good agreement between the analysis and experiment. Once the fundamentals have been verified for single waves at various angles of arrival, one might tend to assume that the technique of superposition is so well known, that further experimental verification is not required. This may not be the case. The scalar analysis neglects certain physical phenomena on the basis of negligible contribution for large apertures and small diffraction angles. Noteworthy is the surface wave generated in the plane of the aperture. We know that the excitation efficiency of this wave increases with increasing angle of arrival. Effects which were insignificant for a single wave may be enhanced by the complex addition with other incident waves. For this reason, it is felt that the focal region fields should be measured for some small number (2 or 3) of incident waves.

One problem, which is very difficult to treat analytically, but which could be exhaustively studied experimentally, is the effect of aperture blocking by the feed assembly. The use of a transmission structure, as the parallel plate lens, has allowed the probing of the diffracted fields without any blockage effect. However, controlled amounts of blockage could be introduced in front of the lens, and the effect determined by field probing. The trends in the perturbation of the diffracted fields would be measured as a function of the size and location of the blockage. Since the effect of the blockage is to produce errors in the aperture plane distribution, these measurements would also provide an indication of how fast the focal region fields degrade with aperture error. It would provide insight as to the number of plane waves required to reasonably approximate typical aperture plane errors.

It is felt that there is now available sufficient data to design an improved feed for a single on-axis wave. This could potentially increase the antenna efficiency by a couple of dB. A small array of properly designed near field feeds could be used to reduce the sidelobe level. The resulting reduction in antenna noise for low noise systems could result in benefits that exceed those predicted by the increase in antenna efficiency.

6. LIST OF CONTRIBUTORS

The following technical personnel performed on this contract:

Dr. Marvin Cohn

Mr. Robert S. Littlepage

APPENDIX

```
C    DIFFRACTION BY A LINEAR APERTURE F/D=.25,
     1D/LAMBDA=50
 3001 FORMAT(15X,F4.1,9X,2(F25.8),F23.4,F25.4)
 3002 FORMAT(*1*,15X,*THETA*,24X,*A*,24X,*B*,24X,*
     1POWER*,20X,*PHASE*)
      PRINT     3002
      THETA=-10.1
      DX=.005
      F=12.5
      D=25.
      THETAP=3.0
      TP=THETAP*.0174523925
      SP=SINF(TP)
      CP=COSF(TP)
      I=0
      PI=3.1415926536
      PI4=PI/4.
      FSQ=F**2
      PI2=2.*PI
      DEL=SQRTF(D**2+FSQ)
   20 I=I+1
      A=0.
      B=0.
      THETA=THETA+.1
      T=THETA*.0174523925
      SN=SINF(T)
      CS=COSF(T)
      TAN=SN/CS
      G1=FSQ/(CS**2)
      FTAN=F*TAN
      X=-D
      XSQ=X**2
      DELTA=DEL-SQRTF(XSQ+FSQ)-X*SP
      G=SQRTF(G1+XSQ-2.*X*FTAN)
      Z=CP+F/G
      TARG=PI2*(G+DELTA)-PI4
      S=SINF(TARG)
      C=COSF(TARG)
      GRT=SQRTF(G)
      AGRND=C*Z/GRT
      BGRND=S*Z/GRT
      DO 100 J = 1,5000
```

```
      X=X+.01
      XSQ=X**2
      DELTA=DEL-SQRTF(XSQ+FSQ)-X*SP
      G=SQRTF(G1+XSQ-2.*X*FTAN)
      Z=CP+F/G
      TARG=PI2*(G+DELTA)-PI4
      S=SINF(TARG)
      C=COSF(TARG)
      AGRNDO=AGRND
      BGRNDO=BGRND
      GRT=SQRTF(G)
      AGRND=C*Z/GRT
      BGRND=S*Z/GRT
      A=A+DX*(AGRND+AGRNDO)
  100 B=B+DX*(BGRND+BGRNDO)
      USQ=.25*(A**2+B**2)
      POWER=10.*ALOG10(USQ)
      PHASE=ATANF(B/A)
      PRINT     3001, THETA, A, B, POWER, PHASE
      IF(I-200)20,20,140
  140 RETURN
      END
```

The parameters in this program are:

THETAP = θ'

F = f/λ

DX = $\frac{\Delta x}{2}$

D = $D/2\lambda$

THETA = θ .

The program presented here computes the single value $\theta' = 3.0^{\circ}$. In actual practice, we used a counting loop to step through θ'.

Unclassified
Security Classification

DOCUMENT CONTROL DATA - R&D

(Security classification of title, body of abstract and indexing annotation must be entered when the overall report is classified)

1. ORIGINATING ACTIVITY *(Corporate author)*
Advanced Technology Corporation
1830 York Road
Timonium, Maryland 21093

2a. REPORT SECURITY CLASSIFICATION
Unclassified

2b. GROUP
---

3. REPORT TITLE
THEORETICAL AND EXPERIMENTAL INVESTIGATION OF FOCAL PLANE ADAPTIVE ANTENNA TECHNIQUES

4. DESCRIPTIVE NOTES *(Type of report and inclusive dates)*
Scientific. Final. 1 April 1967 - 31 March 1968

Approved
14 May 1968

5. AUTHOR(S) *(first name, initial)*, last name
Marvin Cohn
Robert S. Littlepage

6. REPORT DATE	7a. TOTAL NO. OF PAGES	7b. NO. OF REFS
April 1968	76	10

8a. CONTRACT OR GRANT NO.	9a. ORIGINATOR'S REPORT NUMBER(S)
F 19628-67-C-0299	Project No. 50503
b. Project, Task, Work Unit Nos. 4600-10-01, 8683-03-01	
c. DoD Element 62405454, 6240539F	9b. OTHER REPORT NO(S) *(Any other numbers that may be assigned this report)* AFCRL-68-0249
d. DoD Subelement 674600, 681000	

10. AVAILABILITY/LIMITATION NOTICES

1 - Distribution of this document is unlimited. It may be released to the Clearinghouse, Department of Commerce, for sale to the general public.

11. SUPPLEMENTARY NOTES	12. SPONSORING MILITARY ACTIVITY
TECH, OTHER	Air Force Cambridge Research Laboratories (CRD) L. G. Hanscom Field Bedford, Massachusetts 01730

13. ABSTRACT

A scalar analysis has been performed to determine the field structure in the focal region of apertures focused in their near field ($f/D<1$). Solutions are given for plane waves at normal incidence, and several selected angles of arrival. The results indicate a substantial variation from the Fraunhofer far field patterns. Because it is a scalar approach, it is limited to large apertures($D>>\lambda$) and small diffraction angles.

An experiment was designed to complement the analysis. The qualitative agreement is very good. Sources of experimental error have been found which account for the quantitative variations.

A technique for determining the field structure in the focal region, due to a reasonably arbitrary distribution in the aperture plane, is given. It consists of the superposition of an ensemble of plane waves, whose amplitude, relative phase, and angle of arrival are determined by the aperture plane distribution.

DD FORM 1 JAN 64 1473

Unclassified
Security Classification

Unclassified

Security Classification

14. KEY WORDS	LINK A		LINK B		LINK C	
	ROLE	WT	ROLE	WT	ROLE	WT
Antenna						
Diffraction						
Near Field Diffraction						
Adaptive Techniques						
Aperture Function						

INSTRUCTIONS

1. ORIGINATING ACTIVITY: Enter the name and address of the contractor, subcontractor, grantee, Department of Defense activity or other organization *(corporate author)* issuing the report.

2a. REPORT SECURITY CLASSIFICATION: Enter the overall security classification of the report. Indicate whether "Restricted Data" is included. Marking is to be in accordance with appropriate security regulations.

2b. GROUP: Automatic downgrading is specified in DoD Directive 5200.10 and Armed Forces Industrial Manual. Enter the group number. Also, when applicable, show that optional markings have been used for Group 3 and Group 4 as authorized.

3. REPORT TITLE: Enter the complete report title in all capital letters. Titles in all cases should be unclassified. If a meaningful title cannot be selected without classification, show title classification in all capitals in parenthesis immediately following the title.

4. DESCRIPTIVE NOTES: If appropriate, enter the type of report, e.g., interim, progress, summary, annual, or final. Give the inclusive dates when a specific reporting period is covered.

5. AUTHOR(S): Enter the name(s) of author(s) as shown on or in the report. Enter last name, first name, middle initial. If military, show rank and branch of service. The name of the principal author is an absolute minimum requirement.

6. REPORT DATE: Enter the date of the report as day, month, year, or month, year. If more than one date appears on the report, use date of publication.

7a. TOTAL NUMBER OF PAGES: The total page count should follow normal pagination procedures, i.e., enter the number of pages containing information.

7b. NUMBER OF REFERENCES: Enter the total number of references cited in the report.

8a. CONTRACT OR GRANT NUMBER: If appropriate, enter the applicable number of the contract or grant under which the report was written.

8b, 8c, & 8d. PROJECT NUMBER: Enter the appropriate military department identification, such as project number, subproject number, system numbers, task number, etc.

9a. ORIGINATOR'S REPORT NUMBER(S): Enter the official report number by which the document will be identified and controlled by the originating activity. This number must be unique to this report.

9b. OTHER REPORT NUMBER(S): If the report has been assigned any other report numbers *(either by the originator or by the sponsor)*, also enter this number(s).

10. AVAILABILITY/LIMITATION NOTICES: Enter any limitations on further dissemination of the report, other than those imposed by security classification, using standard statements such as:

(1) "Qualified requesters may obtain copies of this report from DDC."

(2) "Foreign announcement and dissemination of this report by DDC is not authorized."

(3) "U. S. Government agencies may obtain copies of this report directly from DDC. Other qualified DDC users shall request through

_____."

(4) "U. S. military agencies may obtain copies of this report directly from DDC. Other qualified users shall request through

_____."

(5) "All distribution of this report is controlled. Qualified DDC users shall request through

_____."

If the report has been furnished to the Office of Technical Services, Department of Commerce, for sale to the public, indicate this fact and enter the price, if known.

11. SUPPLEMENTARY NOTES: Use for additional explanatory notes.

12. SPONSORING MILITARY ACTIVITY: Enter the name of the departmental project office or laboratory sponsoring *(paying for)* the research and development. Include address.

13. ABSTRACT: Enter an abstract giving a brief and factual summary of the document indicative of the report, even though it may also appear elsewhere in the body of the technical report. If additional space is required, a continuation sheet shall be attached.

It is highly desirable that the abstract of classified reports be unclassified. Each paragraph of the abstract shall end with an indication of the military security classification of the information in the paragraph, represented as *(TS), (S), (C), or (U).*

There is no limitation on the length of the abstract. However, the suggested length is from 150 to 225 words.

14. KEY WORDS: Key words are technically meaningful terms or short phrases that characterize a report and may be used as index entries for cataloging the report. Key words must be selected so that no security classification is required. Identifiers, such as equipment model designation, trade name, military project code name, geographic location, may be used as key words but will be followed by an indication of technical context. The assignment of links, rules, and weights is optional.

Unclassified

Security Classification